Running effects on QCD axion phenomenology

Luca Di Luzio[a,b], Maurizio Giannotti[c,d], Federico Mescia[e], Enrico Nardi[f,g], Shohei Okawa[e], Gioacchino Piazza[h,i]

[a]*Istituto Nazionale di Fisica Nucleare (INFN), Sezione di Padova, Via F. Marzolo 8, 35131 Padova, Italy*
[b]*Dipartimento di Fisica e Astronomia 'G. Galilei', Università di Padova, Via F. Marzolo 8, 35131 Padova, Italy*
[c]*Department of Chemistry and Physics, Barry University, 11300 NE 2nd Ave., Miami Shores, FL 33161, USA*
[d]*Centro de Astropartículas y Física de Altas Energías (CAPA), Universidad de Zaragoza, Zaragoza, 50009, Spain*
[e]*Departament de Física Quàntica i Astrofísica, Institut de Ciències del Cosmos (ICCUB), Universitat de Barcelona, Martí i Franquès 1, E-08028 Barcelona, Spain*
[f]*Laboratory of High Energy and Computational Physics, HEPC-NICPB, Rävala 10, 10143 Tallinn, Estonia*
[g]*Istituto Nazionale di Fisica Nucleare, Laboratori Nazionali di Frascati, C.P. 13, 00044 Frascati, Italy*
[h]*IJCLab, Pôle Théorie (Bât. 210), CNRS/IN2P3 et Université Paris-Saclay, 91405 Orsay, France*
[i]*Physik-Institut, Universität Zürich, CH-8057 Zürich, Switzerland*

arXiv:2305.11958v2 [hep-ph] 27 Dec 2023

Abstract

We study the impact of renormalization group effects on QCD axion phenomenology. Focusing on the DFSZ model, we argue that the relevance of running effects for the axion couplings crucially depends on the scale where the heavier Higgs scalars are integrated out. We study the impact of these effects on astrophysical and cosmological bounds as well as on the sensitivity of helioscopes experiments such as IAXO and XENONnT, showing that they can be sizable even in the most conservative case in which the two Higgs doublets remain as light as the TeV scale. We provide simple analytical expressions that accurately fit the numerical solutions of the renormalization group equations as a function of the mass scale of the heavy scalars.

Contents

1 **Introduction** 1

2 **Running QCD axion couplings** 2
2.1 Analytical understanding of RG running effects 3
2.2 DFSZ axion couplings beyond tree level 4

3 **RG effects on QCD axion phenomenology** 5
3.1 Astrophysical constraints 6
3.2 Thermal axion cosmology 9
3.3 Helioscope experiments 9

4 **Conclusions** 11

Appendix A RG equations for DFSZ axion couplings 11

Appendix B Numerical fit to RG effects 13

1. Introduction

Axions are an intrinsic prediction of the Peccei-Quinn (PQ) mechanism [1, 2], which remains, after over four decades, the most appealing solution to the strong CP problem. This problem arises because Quantum Chromodynamics (QCD) predicts CP violating effects that are not observed experimentally. The PQ mechanism involves a new global chiral symmetry $U(1)_{PQ}$, which is anomalous under QCD and spontaneously broken at a large energy scale f_a (PQ scale). The axion is the Nambu-Goldstone boson associated with the spontanous breaking of this symmetry [3, 4], and is characterised by the fact that all its interactions are inversely proportional to f_a. Although the original Weinberg-Wilczek model [3, 4], in which the scale of PQ breaking coincides with the electroweak (EW) symmetry breaking scale, was quickly ruled out, new viable models emerged early on, in which the PQ scale can be arbitrarily high so that all axion interactions can be sufficiently suppressed, yielding the so-called *invisible axion*. Two examples are particularly appealing for their simplicity: the KSVZ or hadronic axion [5, 6] and the DFSZ axion [7, 8]. The main difference between KSVZ and DFSZ-type axions is that the former do not couple to ordinary quarks and leptons at the tree level. Though many other possible axion models have been considered in the literature (see Ref. [9] for a comprehensive overview), the two above-mentioned models are by far the most studied ones and are universally regarded as benchmark QCD axion models. In recent years continuous progress in experimental technologies has brought within reach the possibility of detecting in terrestrial experiments the invisible axions arising in these models. This has stimulated a tremendous interest in this field, with several new theoretical and phenomenological studies, as well as a wealth of new experimental proposals (see [10, 11] for recent reviews). In the meanwhile, ongoing experiments have already started to probe the benchmark KSVZ/DFSZ axion models, and in the coming decades they will dig deep into the relevant parameter space region. From the theory side, this calls for the development of "precision axion physics", which will turn out to be crucial in the case of an axion discovery. Indeed, from a given determination of the low-energy axion couplings to photons and other matter fields (such as electrons and nucleons)

one would like to infer the structure of the high-energy theory, that is the ultraviolet (UV) completion of the axion effective field theory (EFT). This step is highly non-trivial, since it entails a large separation of scales, from the typical low-energy scale of axion experiments up to the PQ scale, $f_a \gtrsim 10^8$ GeV. Hence, axion related physical quantities, as for example the axion couplings to Standard Model (SM) fermions, are potentially affected by large radiative corrections, which can induce large deviations from the tree-level expressions. In the case of the KSVZ model, it was pointed out long ago [12, 13] that although the axion coupling to electrons is zero at tree level, a non-zero electron coupling can be sourced via loop corrections by the axion-photon coupling and, more recently, it was shown that the leading correction to this coupling is generated at even higher orders via the anomalous axion coupling to gluons [14]. Nowadays, the full one-loop anomalous dimensions for the $d = 5$ axion effective Lagrangian have been computed [15–18], while running effects have been investigated for the benchmark DFSZ/KSVZ axion models in Ref. [14], and for the so-called astrophobic axion models (which feature non-universal PQ charges [19, 20]) in Ref. [21].

The purpose of this work is to study QCD axion phenomenology in light of renormalization group (RG) effects, focussing for definiteness on the mass window $m_a \in [\text{meV}, \text{eV}]$. This region of parameter space shows a remarkable complementarity among the existing bounds on the different axion couplings, namely to photons, electrons, nucleons and pions, stemming from helioscope searches, as well as from astrophysics and cosmology. It is therefore an ideal playground where to investigate the consequences of running effects for QCD axion phenomenology. In particular, we will focus on the large corrections induced by the top Yukawa coupling, which apply to a large class of axion models where the SM fermions are charged under the $\text{U}(1)_{\text{PQ}}$ symmetry. A paradigmatic example is the universal DFSZ model, which features two Higgs doublets and one SM singlet scalar, and whose axion parameter space at tree level depends solely on m_a and $\tan\beta$. However, top-Yukawa radiative corrections induce a logarithmic dependence of the effective axion couplings on the mass scale of the heavy scalar degrees of freedom of the two Higgs doublet model (2HDM) (the issue of large logarithmic corrections is well known in the 2HDM literature, see e.g. [22, 23]) that can range from about 1 TeV up to the PQ scale, f_a. As we shall see, these corrections are often large and may skew the parameter space region that is effectively probed by terrestrial experiments and by astrophysical/cosmological observations.

The paper is organized as follows. In Sect. 2 we discuss the structure of top-Yukawa radiative corrections, and we provide approximate analytical expressions for the dependence of the axion couplings on these corrections. Sect. 3 is devoted to study the impact of running effects on QCD axion phenomenology, including the consequences for astrophysical and cosmological limits as well as for the sensitivity of future axion experiments. We conclude in Sect. 4. Details on the solutions to the RG equations are provided in Appendix B.

2. Running QCD axion couplings

Of central interest for axion phenomenology are the axion couplings to photons and matter fields (electrons, nucleons, as well as other hadrons relevant for axion production). They are defined by the following interaction Lagrangian:

$$\begin{aligned}\mathcal{L}_a = {} & C_\gamma \frac{\alpha}{8\pi}\frac{a}{f_a} F^{\mu\nu}\tilde{F}_{\mu\nu} + \sum_{f=p,n,e} C_f \frac{\partial_\mu a}{2f_a}\bar{f}\gamma^\mu\gamma_5 f \\ & + C_\pi \frac{\partial_\mu a}{f_a f_\pi}(2\partial^\mu\pi^0\pi^+\pi^- - \pi^0\partial^\mu\pi^+\pi^- - \pi^0\pi^+\partial^\mu\pi^-) \\ & + C_{\pi N}\frac{\partial_\mu a}{2f_a f_\pi}(i\pi^+\bar{p}\gamma^\mu n - i\pi^-\bar{n}\gamma^\mu p) \\ & + C_{N\Delta}\frac{\partial^\mu a}{2f_a}\left(\bar{p}\,\Delta^+_\mu + \overline{\Delta^+_\mu}\,p + \bar{n}\,\Delta^0_\mu + \overline{\Delta^0_\mu}\,n\right) + \dots\,, \end{aligned} \tag{1}$$

where $F_{\mu\nu}$ denotes the electromagnetic field strength, $\tilde{F}_{\mu\nu} = \frac{1}{2}\epsilon_{\mu\nu\rho\sigma}F^{\rho\sigma}$ (with $\epsilon^{0123} = -1$) its dual, $f = p, n, e$ runs over low-energy matter fields, and $C_{\gamma,f,\pi,\pi N,N\Delta}$ are $O(1)$ dimensionless coefficients. The axion-pion coupling in the second line of Eq. (1) (with $f_\pi = 92.1(8)$ MeV [24] the pion decay constant) is of phenomenological relevance for thermal axion production in the early Universe, while the axion contact interactions with pions and nucleons (third line) and with Δ-resonances (fourth line) are important for axion production in Supernovae (SNe). The ellipses stand for other possible axion interaction terms which will not be considered in this paper.

In the context of axion phenomenology, one usually employs the dimensional couplings $g_{a\gamma} = \frac{\alpha}{2\pi}C_\gamma/f_a$ and $g_{af} = C_f\, m_f/f_a$. In particular, $C_\gamma = E/N - 1.92(4)$, where E/N is the ratio between the electromagnetic and QCD anomalies of the PQ current (for typical values in concrete axion models, see e.g. [25, 26]). Note that to a very good approximation the anomalous axion-photon coupling is insensitive to running effects, with first corrections appearing at three loops [17]. Moreover, mass dependent corrections to the effective axion-photon coupling are safely negligible for $m_a \ll m_e$ since they scale at most as $(m_a/m_e)^2$ – see e.g. Ref. [27]. Hence, in the following, we will only focus on radiative corrections to the axion couplings to electrons and hadrons.

Axion-hadron interactions can be expressed in terms of the model-independent axion gluon coupling (which fixes the absolute normalization in terms of f_a) and the axion couplings to quark fields, $q = u, d, s, c, b, t$, defined via the Lagrangian term[1]

$$C_q \frac{\partial_\mu a}{2f_a}\bar{q}\gamma^\mu\gamma_5 q\,. \tag{2}$$

In terms of the latter, the axion couplings to hadrons defined in

[1] In this work we focus on universal axion models, so that the axial-vector currents in Eq. (2) are flavor diagonal. However, as long as the PQ charges of different generations are not hierarchical, most of the considerations related to top-Yukawa running effects, to be discussed below, apply as well to non-universal axion models (see e.g. Ref. [21]).

Eq. (1) read (see e.g. [9, 28–30])

$$C_p = C_u\Delta_u + C_d\Delta_d + C_s\Delta_s - \left(\frac{\Delta_u}{1+z} + \frac{z\,\Delta_d}{1+z}\right), \quad (3)$$

$$C_n = C_d\Delta_u + C_u\Delta_d + C_s\Delta_s - \left(\frac{z\,\Delta_u}{1+z} + \frac{\Delta_d}{1+z}\right), \quad (4)$$

$$C_\pi = -\frac{1}{3}\left(C_u - C_d - \frac{1-z}{1+z}\right), \quad (5)$$

$$C_{\pi N} = -\frac{3}{\sqrt{2}}C_\pi\,, \qquad C_{N\Delta} = \frac{3\sqrt{3}}{2}C_\pi\, g_A\,, \quad (6)$$

where $C_{u,d,s} = C_{u,d,s}(2\,\text{GeV})$ are low-energy couplings evaluated at the scale $\mu = 2\,\text{GeV}$ by numerically solving the RG equations from the boundary values $C_{u,d,s}(f_a)$ (see below), $\Delta_{u,d,s}$ denote the nucleon matrix elements of the quark axial-vector currents. In particular, $g_A \equiv \Delta_u - \Delta_d = 1.2754(13)$ from β-decays [24], $\Delta_u = 0.847(18)(32)$, $\Delta_d = -0.407(16)(18)$ and $\Delta_s = -0.035(6)(7)$ (at 2 GeV in the $\overline{\text{MS}}$ scheme) are the $N_f = 2+1$ FLAG average [31], that is dominated by the results of [32], and $z = m_u(2\,\text{GeV})/m_d(2\,\text{GeV}) = 0.49(2)$ [33]. Combining lattice values with the high-precision determination of g_A, we obtain the weighted averages $\Delta_u = 0.858(22)$, $\Delta_d = -0.418(22)$ and $\Delta_s = -0.035(9)$.

Running effects on the low-energy couplings of the axion to first generation SM fermions can be parametrized as[2] (see e.g. [14])

$$C_u(2\,\text{GeV}) = C_u(f_a) + \Delta C_u\,, \quad (7)$$

$$C_d(2\,\text{GeV}) = C_d(f_a) + \Delta C_d\,, \quad (8)$$

$$C_e(m_e) = C_e(f_a) + \Delta C_e\,, \quad (9)$$

with

$$\Delta C_\Psi \simeq r^t_\Psi(m_{\text{BSM}})\; C_t(f_a)\,, \quad (10)$$

and $\Psi = u, d, e$. The parameter $r^t_\Psi(m_{\text{BSM}})$ encodes the RG correction approximated by taking only the top-Yukawa contribution, and depends logarithmically on the parameter $m_{\text{BSM}} \simeq m_{H,A,H^+}$ that denotes collectively the mass scale of the heavy scalar degrees of freedom (we implicitly assume for the heavy modes of the scalar doublets the decoupling limit [34], in which all the heavy masses are approximately degenerate). The m_{BSM} scale depends on the structure of the DFSZ scalar potential, whose details (see e.g. [35, 36]) are not crucial for the calculation of the axion RG equations, and we take it to range from about 1 TeV (the approximate lower bound as set by LHC searches for new heavy scalars) up to f_a.

Note that as long as the couplings are considered at a renormalization scale μ above m_{BSM} there are no top-Yukawa running effects. This is because in this regime the axion couplings to the SM fermions correspond to the global charges of the PQ current, which is classically conserved, and thus they do not renormalize. For $\mu < m_{\text{BSM}}$ we enter a different regime, in which Higgs doublets with different PQ charges mix to give rise to heavy scalars (which are integrated out) and to the light Higgs, that has no well-defined charge. In this effective theory there is no more a conserved PQ current, and running effects for the axion-fermion couplings can kick in. This is the reason why the largest RG effects appear when the BSM scale is taken at the largest possible scale $m_{\text{BSM}} \sim f_a$. Contrary, when the 2HDM structure keeps holding all the way down to the TeV scale, running effects are much less sizeable.

In Appendix B we provide a fit to $r^t_\Psi(m_{\text{BSM}})$ obtained by interpolating the numerical solution to the RG equations (cf. Eqs. (B.6)-(B.7) and Tab. B.4). Taking, for instance, $m_{\text{BSM}} = f_a = 10^{10}$ GeV one finds

$$C_u(2\,\text{GeV}) \simeq C_u(f_a) - 0.264\,C_t(f_a)\,, \quad (11)$$

$$C_d(2\,\text{GeV}) \simeq C_d(f_a) + 0.266\,C_t(f_a)\,, \quad (12)$$

$$C_e(m_e) \simeq C_e(f_a) + 0.265\,C_t(f_a)\,. \quad (13)$$

2.1. Analytical understanding of RG running effects

To understand the phenomenological impact of the RG corrections to the axion couplings, and to compare it with the current experimental sensitivity, it is convenient to provide some analytical approximations. To this aim, it is advantageous to introduce the iso-scalar (C_0) and iso-vector (C_3) nuclear couplings (see also [21]), defined as follows:

$$C_0 = \frac{1}{2}\Big(C_p + C_n\Big) = \frac{1}{2}(\Delta_u + \Delta_d)(C_u + C_d - 1) - \Delta_s C_s\,, \quad (14)$$

$$C_3 = \frac{1}{2}(C_p - C_n) = \frac{g_A}{2}\left(C_u - C_d - \frac{1-z}{1+z}\right), \quad (15)$$

where the right-hand sides are obtained from the expressions for $C_{p,n}$ given in Eqs. (3)-(4). From Eqs. (5)-(6) we see that all the other couplings are proportional to the iso-vector combination C_3: $C_\pi = -\frac{2}{3}\,g_A^{-1}C_3$, $C_{\pi N} = \sqrt{2}\,g_A^{-1}\,C_3$, $C_{N\Delta} = -\sqrt{3}\,C_3$.

The RG correction to the iso-vector combination $\Delta C_3 \simeq 0.64\,C_t(f_a)\,(r^t_u - r^t_d)$ may be sizeable, with the exact value depending on the m_{BSM} scale. An excellent fit to the combination $r^t_u - r^t_d$, for m_{BSM} in the range 1 TeV to 10^{18} GeV, is given by

$$r^t_u - r^t_d \approx -0.54\,\ln\Big(\sqrt{x} - 0.52\Big), \quad (16)$$

with $x = \log_{10}(m_{\text{BSM}}/\text{GeV})$. This expression reproduces our numerical results with a precision better than 2% (see Appendix B). Then, in the relevant range for m_{BSM}, we have $0.3 \lesssim |r^t_u - r^t_d| \lesssim 1$. Since in universal axion models we expect $C_3 \sim C_t$ (the exact relation depending on the model parameters), we can conclude that $\Delta C_3/C_3$ can be of the order of a few 10%, and even larger. For example, in the case of the DFSZ axion (to be discussed below), we find

$$\left|\frac{\Delta C_3}{C_3}\right|_{\text{DFSZ}} \simeq \frac{0.5}{\tan\beta}\left(r^t_u - r^t_d\right) + O\Big((r^t_d - r^t_u)^2\Big), \quad (17)$$

which can become quite significant at small $\tan\beta$.

On the other hand, the RG correction to the iso-scalar coupling C_0 is, in general, very small. From Eq. (14), we see that this coupling combination gets contributions from $(r^t_u + r^t_d)$ and from $\Delta_s C_s$. As it was pointed out in Ref. [21], in the leading approximation in which only the contribution of the top-quark

[2] In universal axion models the same corrections apply to each generation.

Yukawa coupling is kept, the combination $(r_u^t + r_d^t)$ is characterized by a strong cancellation, see for example Eqs. (11)-(12), and is numerically very small $\sim 0.2\%$.[3] Hence, eventually the leading correction to C_0 comes from the RG correction $\Delta_s \Delta C_s$ to the last term in Eq. (14). It is easy to estimate this contribution from our general results, using $r_s^t = r_d^t$ that holds for universal models. In the end, we find that the RG corrections to C_0 are only about 3% of the corresponding corrections to C_3 and hence this combination of couplings (and the corresponding iso-scalar axion coupling to nucleons, $g_{aN,0} = C_0 m_N / f_a$) is practically unaffected by RG running effects.

2.2. DFSZ axion couplings beyond tree level

The scalar sector of DFSZ models [7, 8] features a SM singlet complex scalar Φ and two Higgs doublets $H_{u,d}$ that couple respectively to up- and down-type quarks in a generation-independent way. Under $\mathrm{SU}(3)_C \times \mathrm{SU}(2)_L \times \mathrm{U}(1)_Y$ they transform as $\Phi \sim (1,1,0)$, $H_u \sim (1,2,-1/2)$ and $H_d \sim (1,2,1/2)$. The threefold re-phasing symmetry of the scalar sector $\mathrm{U}(1)_\Phi \times \mathrm{U}(1)_{H_u} \times \mathrm{U}(1)_{H_d}$ is broken to $\mathrm{U}(1)_{\rm PQ} \times \mathrm{U}(1)_Y$ by a renormalizable non-Hermitian operator that can be chosen as $H_u H_d \Phi^{\dagger 2}$ or $H_u H_d \Phi^\dagger$.[4] There are two possible variants of the model, depending on whether the lepton sector couples to H_d (DFSZ1) or to $\tilde{H}_u = i\sigma^2 H_u^*$ (DFSZ2). For a review see Sec. 2.7.2 in Ref. [9]. The Yukawa sector of the DFSZ1 model contains the following operators

$$\bar{q}_i u_j H_u \,, \quad \bar{q}_i d_j H_d \,, \quad \bar{\ell}_i e_j H_d \,, \tag{18}$$

where a sum over generation indices $i, j = 1,2,3$ is left understood, and q_i, ℓ_i denote the quarks and leptons $\mathrm{SU}(2)_L$ left-handed (LH) doublets while u_j, d_j, e_j the right-handed (RH) singlets. The corresponding coefficients for the axion coupling at the UV scale f_a are

$$\frac{E}{N} = \frac{8}{3} \,, \quad C_{u,c,t}(f_a) = \frac{c_\beta^2}{3} \,, \quad C_{d,s,b}(f_a) = C_{e,\mu,\tau}(f_a) = \frac{s_\beta^2}{3} \,, \tag{19}$$

with $c_\beta \equiv \cos\beta$, $s_\beta \equiv \sin\beta$ and $\tan\beta = \langle H_u \rangle / \langle H_d \rangle \equiv v_u / v_d$. The domain in which $\tan\beta$ is allowed to vary is obtained by requiring that the DFSZ Yukawas remain perturbative up to scales of $O(f_a)$. This corresponds to imposing perturbative unitarity on Higgs-mediated $2 \to 2$ SM fermion scatterings (see e.g. [37]) up to f_a. The perturbative domain is evaluated by evolving the values of the gauge couplings and of the SM Yukawa couplings at m_Z given in Ref. [38] up to the scale $m_{\rm BSM}$ employing two-loop RG equations.

For $m_{\rm BSM} \sim f_a$ the SM Yukawa couplings are RG-evolved from m_Z to f_a, and upon matching with the DFSZ couplings $Y_t^{\rm DFSZ} = Y_t(f_a)/s_\beta$ and $Y_b^{\rm DFSZ} = Y_b(f_a)/c_\beta$, by requiring $Y_{t,b}^{\rm DFSZ} < \sqrt{16\pi/3}$ [9]. This yields the perturbative domain

$$\tan\beta \in [0.14, 500] \qquad (m_{\rm BSM} \sim f_a \sim 10^9 \text{ GeV}) \,, \tag{20}$$

[3] From the more accurate numerical analysis in Appendix B we obtain that for any value of the $m_{\rm BSM}$ scale $|r_u^t + r_d^t| / |r_u^t - r_d^t| \lesssim 0.5\%$.

[4] The first possibility yields a number of domain walls $N_{\rm DW} = 6$ while the second $N_{\rm DW} = 3$, but they remain otherwise indistinguishable from the point of view of low-energy phenomenology.

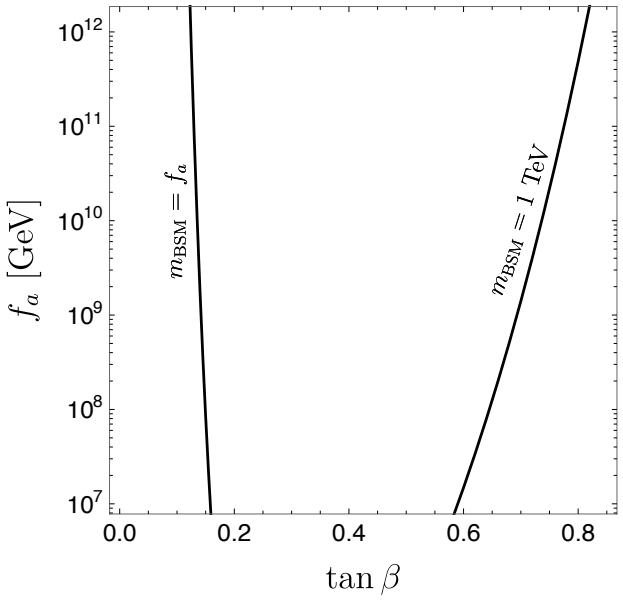


Figure 1: f_a dependence of the perturbative unitarity bounds on $\tan\beta$ at small $\tan\beta$ values.

On the other hand, for $m_{\rm BSM} \ll f_a$ one should require a stronger perturbativity constraint on $Y_{t,b}^{\rm DFSZ}$, since running effects from $m_{\rm BSM}$ to f_a would tend to develop Landau poles in the DFSZ Yukawa couplings below f_a. In this case $Y_{t,b}$ are evolved from m_Z to $m_{\rm BSM}$ within the SM, and after matching with the DFSZ couplings $Y_t^{\rm DFSZ}(m_{\rm BSM}) = Y_t(m_{\rm BSM})/s_\beta$ and $Y_b^{\rm DFSZ}(m_{\rm BSM}) = Y_b(m_{\rm BSM})/c_\beta$, the running of $Y_{t,b}^{\rm DFSZ}$ from $m_{\rm BSM}$ to f_a is computed in the 2HDM. In the case when $m_{\rm BSM} \sim 1$ TeV perturbative unitarity up to $f_a \sim 10^9$ GeV translates in the following interval

$$\tan\beta \in [0.70, 100] \qquad (m_{\rm BSM} \sim 1 \text{ TeV}) \,. \tag{21}$$

Note that the perturbative domain of $\tan\beta$ has a mild (logarithmic) dependence on the PQ scale f_a. This is shown in Fig. 1 for the low $\tan\beta$ region (a similar dependence is present also for the large $\tan\beta$ region, where running effects are however less important).

The Yukawa sector of the DFSZ2 model contains instead the following operators

$$\bar{q}_i u_j H_u \,, \quad \bar{q}_i d_j H_d \,, \quad \bar{\ell}_i e_j \tilde{H}_u \,, \tag{22}$$

and the corresponding axion coupling coefficients are

$$\frac{E}{N} = \frac{2}{3} \,, \quad C_{u,c,t}(f_a) = -C_{e,\mu,\tau}(f_a) = \frac{c_\beta^2}{3} \,, \quad C_{d,s,b}(f_a) = \frac{s_\beta^2}{3} \,, \tag{23}$$

with $\tan\beta$ defined in the same perturbative domain as in DFSZ1.

Let us now proceed to discuss the impact of running effects in the DFSZ model. Approximate RG corrections to the axion couplings are collected in Tab. 1. Note that in the case of DFSZ1 the iso-vector combination C_3, as well as the axion-electron coupling C_e, receive large corrections at small $\tan\beta$,

Coupling (DFSZ1)	Coupling (DFSZ2)	Approximate Correction
$C_0 \simeq -0.20$	$C_0 \simeq -0.20$	$\Delta C_0 \approx 0$
$C_3 \simeq -0.43\ \sin^2\beta$	$C_3 \simeq -0.43\ \sin^2\beta$	$\Delta C_3 \simeq -0.12\, l(x)\ \cos^2\beta$
$C_e = \frac{1}{3}\sin^2\beta$	$C_e = -\frac{1}{3}\cos^2\beta$	$\Delta C_e \simeq 0.094\, l(x)\ \cos^2\beta$
$C_\gamma = \frac{8}{3} - 1.92$	$C_\gamma = \frac{2}{3} - 1.92$	$\Delta C_\gamma = 0$

Table 1: RG corrections (third column) to the DFSZ1 and DFSZ2 couplings (listed respectively in the first and second column) in the approximation of keeping only the contribution from the top Yukawa coupling Y_t. The corrections are given in terms of β and of $l(x) = \ln(\sqrt{x} - 0.52)$, where $x = \log_{10}(m_{\rm BSM}/{\rm GeV})$ parameterizes the new physics scale. While the corrections to the quark couplings in DFSZ1/2 are the same, for the leptons the relative corrections differ: $\Delta C_e/C_e \simeq \cot^2\beta$ (DFSZ1) and $\Delta C_e/C_e \simeq$ const. (DFSZ2).

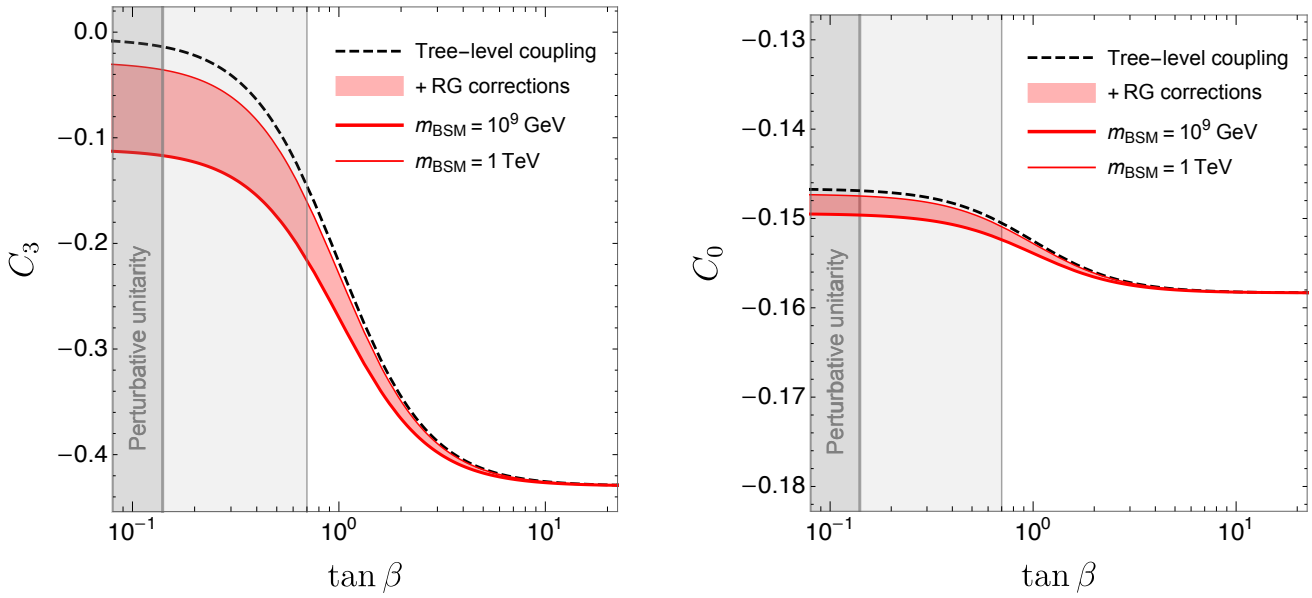


Figure 2: Running axion coupling combinations (C_3 and C_0) in DFSZ as a function of $\tan\beta$. The red band encompasses the range of the corrections for $m_{\rm BSM}/{\rm GeV} \in [10^3, 10^9]$. Perturbativity bounds on $\tan\beta$ also depend on $m_{\rm BSM}$, with the thick (thin) grey line corresponding to $m_{\rm BSM} = 10^9$ GeV (1 TeV).

that is when the tree-level coupling vanishes.[5] On the other hand, the RG corrections on the iso-scalar combination C_0 remain small in the whole $\tan\beta$ range. This is also displayed in Fig. 2, where the dashed line corresponds to the tree-level result, while the red band encodes the range of RG corrections obtained by varying $m_{\rm BSM}$ between $f_a = 10^9$ GeV (lower border of the red region) and 1 TeV (upper border of the red region). We see that although for $m_{\rm BSM} = 1$ TeV the running couplings trace closely the tree-level couplings as long as $\tan\beta > 1$, also in this case RG corrections become non-negligible at small $\tan\beta$.

3. RG effects on QCD axion phenomenology

In the following section, we will discuss the phenomenological impacts of the RG corrections. In particular, we will see how these affect axion astrophysical and cosmological bounds, as well as the sensitivity of terrestrial experimental searches. For clarity, we will refer to the DFSZ axion models, even though our results can be applied to other axion models.

Several observables depend dominantly (or entirely) on C_3 and thus, as discussed in Sect. 2, are subjected to large RG-induced modifications. These include for example the coupling to pions, which is responsible for the axion thermalization in the early Universe (via $\pi\pi \leftrightarrow \pi a$), which controls the hot dark matter (HDM) bound discussed in Sect. 3.2. More recently, it has also been shown that the pion-nucleon scattering may be responsible for a large contribution to the axion emission rates in dense media, particularly in SNe [39–41]. Finally, the iso-vector coupling C_3 is entirely responsible for the nuclear reaction process $p + d \to {}^3{\rm He} + a$, which is one of the most efficient and widely studied production mechanisms of axion-like particles from solar nuclear reactions [42–46]. On the other hand, the nucleon coupling to ^{57}Fe, relevant for axion production through nuclear de-excitations in the Sun [42, 43, 47], turns out to be less sensitive to RG corrections (see Tab. 2).

The axion-electron coupling C_e, which plays a significant role in astrophysics (see Section 3.1) as well as in terrestrial experimental searches (see Section 3.3), is also subjected to large RG corrections. In fact, $r_e^t \approx r_d^t$.[6] Thus, using $r_u^t + r_d^t \approx 0$ and

[5] Note that the suppression of C_3 at small $\tan\beta$ arises due to an accidental cancellation between $C_u - C_d$ and the quark mass term, cf. Eq. (15).

[6] This conclusion is based on the same arguments presented above, where

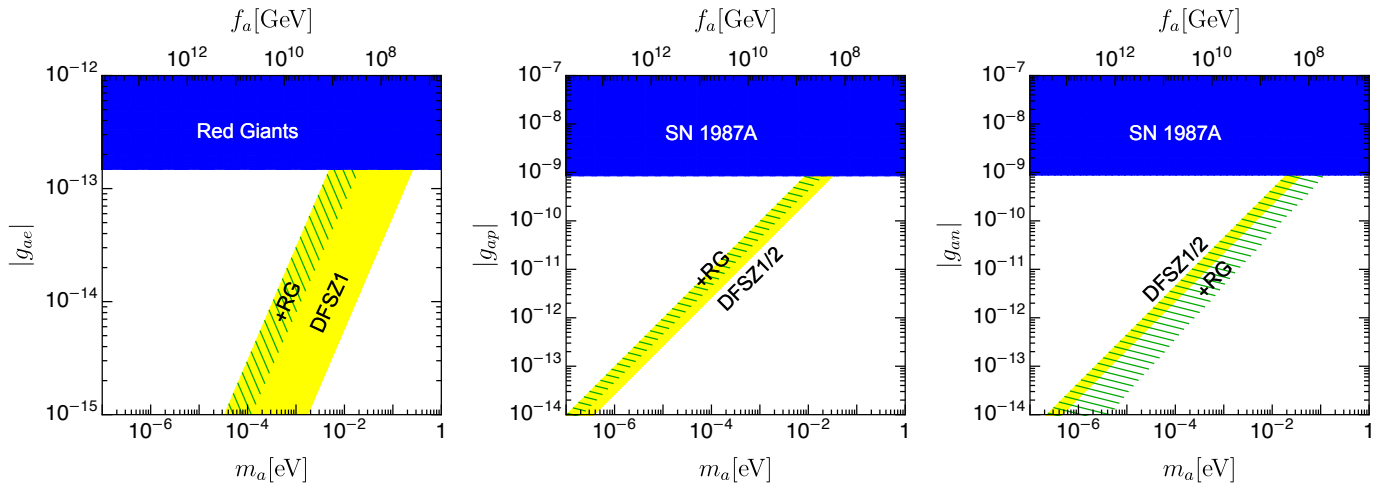


Figure 3: Redefinition of the predicted bands for the DFSZ couplings $g_{ae}^{\rm DFSZ1}$ (left), $g_{ap}^{\rm DFSZ1/2}$ (middle), and $g_{an}^{\rm DFSZ1/2}$ (right) induced by RG effects (hatched green region). The size of the band correspond the perturbativity unitarity bounds on $\tan\beta$ (see text). The $m_{\rm BSM}$ new physics scale is set to the maximal value $m_{\rm BSM} = f_a$.

Eq. (16), we find

$$r_e^t \simeq -\frac{1}{2}\left(r_u^t - r_d^t\right) \approx 0.27\ln\left(\sqrt{x} - 0.52\right), \qquad (24)$$

where $x = \log_{10}(m_{\rm BSM}/{\rm GeV})$ parameterizes the new physics scale.[7] Therefore the corrections to C_e can also be expressed in terms of ΔC_3. Specifically, from our previous results we see that $\Delta C_e = -0.5\, C_t(f_a)\,(r_u^t - r_d^t) = -0.78\,\Delta C_3$. Thus, at our level of approximation all running effects can be expressed in terms of ΔC_3, which for DFSZ axions is $\propto \cos^2\beta$. A general consequence of this observation is that, in the case of DFSZ axions, the running effects are mostly relevant only at small $\tan\beta$, something that is apparent from our numerical analysis.[8]

Before moving to the phenomenological study, it is instructive to anticipate how RG corrections will modify the usual DFSZ bands, obtained by varying the value of $\tan\beta$ within the perturbative unitarity limits, for the g_{ae}, g_{ap}, g_{an} couplings (see for example the section on axions in the Review of Particle Physics [48]). This can be easily estimated by considering the RG corrections to the electron and to the nucleon couplings $C_{p,n} = C_0 \pm C_3$ given in Table 1. The results are shown in Fig. 3, where we have taken $m_{\rm BSM} = f_a \propto 1/m_a$ to maximize the RG effects. In each panel the bands correspond to varying $\tan\beta$ in the interval $[0.14, 100]$. The first figure shows the modification of the usual g_{ae} band in DFSZ1. For this case we obtain the most dramatic effect, that is a marked reduction of the width of the band that, after including RG corrections, shrinks down to the green hatched region. This is due to the fact that the tree-level suppression of $g_{ae}^{\rm DFSZ1}$ in the limit $\sin\beta \to 0$ is cut-off at small $\tan\beta$ by the RG correction proportional to $\cos^2\beta$. Instead there is not such a dramatic effect for $g_{ae}^{\rm DFSZ2}$ since both the tree level coupling and the RG correction are proportional to $\cos^2\beta$. In the second panel in Fig. 3 we show the RG effect on the band for g_{ap} (that is the same in DFSZ1 and in DFSZ2). In this case we see that the shrinking of the allowed band is much less pronounced. Finally, the third panel shows the RG effects on the g_{an} band. In this case the allowed band is sizeably widened, which this is due to a cancellation in the $\tan\beta$ independent part of the coupling, which enhances the overall dependence on this parameter.

The most important phenomenological consequences of the RG corrections to the axion couplings will be analyzed in the following sections.

3.1. Astrophysical constraints

In this Section, we discuss the impact of RG corrections to astrophysical observables. For reference, we will mostly focus on the DFSZ1 axion model. The analysis for DFSZ2 goes along similar lines.

Axions can be copiously produced in stars, mostly due to thermal processes (see Ref. [53] for a recent review). Here we will not consider astrophysical bounds on the axion-photon coupling [60–63], since C_γ does not receive any relevant RG correction. We focus instead on the axion-electron and on the axion-nucleon couplings.

The most stringent astrophysical bound on the axion-electron coupling is derived from observations of the tip of the red giant branch (RGB) in globular clusters. The production of axions during the RGB evolution cools the core, playing a role similar to that of neutrinos, and thus delays the helium ignition. The delay leads to a larger helium core and, consequently, to a higher stellar luminosity. Thus, comparison between observations and predictions for the luminosity of the RGB tip (the brightest stars in the RGB) is an efficient way to test anomalous channels of stellar cooling. The most recent analysis has set the constraint $|g_{ae}| \leq 1.48 \times 10^{-13}$ (at 95% C.L.) [64]. From the definition of

it was argued that $r_u^t + r_d^t \simeq 0$. Deviations from these relations are due to subleading contributions of Yukawa terms other than Y_t. A detailed discussion can be found in Section 3 of Ref. [21].

[7] This result should not be surprising since it holds in the limit of $|r_u^t + r_d^t| \approx 0$ and, as discussed above, $|r_u^t + r_d^t|/|r_u^t - r_d^t| \lesssim 0.5\%$.

[8] The only exception is in cases where the $\cos\beta$ dependence cancels, as for $\Delta C_e/C_e$ in the DFSZ2 model (see the Red Giant bound on DFSZ2 axion in the right panel of Fig. 4).

Coupling	Approximate Correction	Processes
C_0	$\Delta C_0 \approx 0$	
C_3	$\Delta C_3 \simeq 0.64\, C_t(f_a)\,(r_u^t - r_d^t)$	Axion thermalization: $\pi\pi \leftrightarrow \pi a$ [13, 49–52] Deuteron processes: $p + n \leftrightarrow d + a$ [44–46]
$C_p = C_0 + C_3$	$\Delta C_p \approx \Delta C_3$	Astrophysics/experiments [10, 11, 53]
$C_n = C_0 - C_3$	$\Delta C_n \approx -\Delta C_3$	Astrophysics/NMR experiments [54, 55]
$C_{\rm SN} \simeq 1.4\Big(C_0^2 + 0.11\, C_0 C_3 + 1.3\, C_3^2\Big)^{1/2}$,	$\Delta C_{\rm SN} \simeq (2.5\, C_3 + 0.11\, C_0)\frac{\Delta C_3}{C_{\rm SN}}$.	SN 1987A bound [41]
$C_{\rm Fe} = C_0 - 0.77\, C_3$	$\Delta C_{\rm Fe} = -0.77 \Delta C_3$	Axion production/detection in ^{57}Fe [42, 43, 47]
C_e	$\Delta C_e = -0.78\, \Delta C_3$	Axion production in stars [53] Axion detection (Xenon etc.) [56–58]
C_γ	$\Delta C_\gamma = 0$	Axion production in stars and labs [9] Most axion detection experiments [10, 11]
$C_{\rm hel} = \Big[C_\gamma^2\Big(C_\gamma^2 + (37 C_e)^2\Big)\Big]^{1/4}$	$\Delta C_{\rm hel} = \dfrac{C_{\rm hel}}{2}\left(\dfrac{\Delta C_e/C_e}{1 + \Big(C_\gamma/(37 C_e)\Big)^2}\right)$	Axion coupling for Sikivie helioscopes [9, 59]

Table 2: RG corrections (second column) to axion couplings listed in the first column, in the approximation of keeping only the contribution from the top Yukawa coupling Y_t. Note that in this approximation all the various corrections can be expressed just in terms of ΔC_3 given in the second line, with $r_u^t - r_d^t$ given in Eq. (16).

this coupling, $g_{ae} = C_e m_e / f_a$, the RGB bound translates into

$$|C_e| \leq 1.65 \times 10^{-3} \left(\frac{m_a}{\rm eV}\right)^{-1} . \tag{25}$$

This relation provides an upper bound for the axion mass at any given value of $\tan\beta$ and $x = \log_{10}(m_{\rm BSM}/{\rm GeV})$. The full numerical results are shown in Fig. 4, where the red-shaded bands incorporate the range fixed by the possible values of $m_{\rm BSM} \in [1\ {\rm TeV}, f_a]$.

We can gain some intuition about these effects using our approximate results, shown in Table. 1. In the case of the DFSZ1 model (left panel in Fig. 4) we can conveniently rewrite the RGB bound on the axion mass as follows[9]

$$\left(\frac{m_a}{\rm eV}\right) \leq \frac{1.65 \times 10^{-3}}{\left|\left(\frac{1}{3} - 0.094\, l(x)\right)\sin^2\beta + 0.094\, l(x)\right|} , \tag{26}$$

where $l(x) = \ln\Big(\sqrt{x} - 0.52\Big)$. The first important observation is that in the limit $l(x) \to 0$, that is ignoring the RG corrections, the RGB bound on the mass is a monotonic function of $\tan\beta$ and disappears in the limit of small $\tan\beta$. This result is modified by the RG corrections, which in the limit $\tan\beta \to 0$ still provide a useful limit on the axion mass, $m_a \leq 0.018\,{\rm eV}/l(x)$. From these considerations, we can conclude that the RG correction to the RGB bound becomes particularly important in the low $\tan\beta$ limit, a result confirmed by the full numerical result shown in Fig. 4. The most conservative value for the RGB bound corresponds to $m_{\rm BSM} = 1\,{\rm TeV}$, for which we obtain, in our approximation, $m_a \leq 0.018\,{\rm eV}/l(3) \simeq 8.75\times10^{-2}\,{\rm eV}$, which agrees well with the complete numerical result shown in the left panel of Fig. 4. In the case of the DFSZ2 model instead, there is not such a striking feature, and this is because in this case both the coupling g_{ae} and its RG correction depend on $\cos\beta$. The RGB bound for this case is shown in the right panel of Fig. 4.

Let us now move to the axion-nucleon coupling and analyze the axion bound from SN1987A.[10] This is a quite more complex problem since axion production in a SN environment, at temperatures of order $\sim 30\,{\rm MeV}$ and densities in excess of $\sim 10^{14}\,{\rm g/cm^3}$, gets contributions also from pions [29, 39, 40] and from Δ baryon resonances [30]. Following the notation of Ref. [41], the effective low-energy axion-nucleon interaction relevant for the axion production processes in a SN environment is given in Eq. (1). The second term in the first line describes the usual axion-nucleons interactions. The third line contains the axion-pion interactions. The four-particle interaction vertex in the third line accounts for the pion-nucleon contact term recently discussed in Ref. [29], while the last line accounts for the axion couplings to the Δ-resonances, whose contribution to the axion emissivity has been recently calculated in Ref. [30]. The interaction Lagrangian in Eq. (1) can be used to compute the axion emissivity due to nucleon-nucleon (NN) bremsstrahlung, $NN \to NNa$, as well as the Compton-like pion scattering processes, $\pi^- p \to na$, including also the contribution from the Δ resonances (see Ref. [41] for an updated overview).

In general, the axion luminosity from a SN, L_a, depends only

[9] Notice that in the range of $m_{\rm BSM}$ we are considering here, the absolute value in Eq. (26) is unnecessary.

[10] SN1987A is not the only astrophysical probe of the axion-nucleon coupling. Neutron stars also provide strong bounds (see, e.g., Ref. [65]). However, the bound from SN1987A is the most discussed in the literature, and thus it provides a good example for the impact of RG corrections.

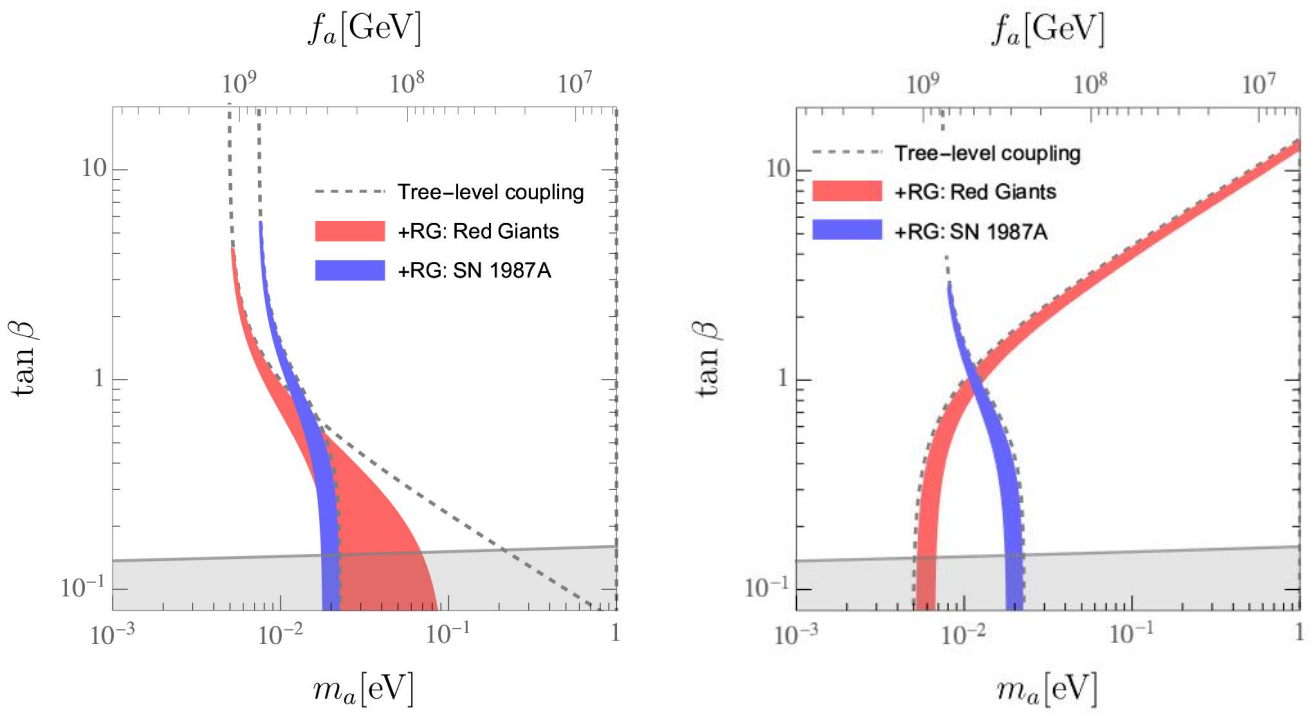


Figure 4: RG effects on astrophysical axion bounds from Red Giants (red bands) and SN1987A (blue bands) for the DFSZ1 (left panel) and DFSZ2 (right panel) models, compared to the tree level results (black dashed lines). The gray line corresponds to the perturbative unitarity bound on $\tan\beta$ for $m_{\rm BSM} = f_a$.

	ϵ_0	a	b	c	$\overline{m}$ [meV]
NN	2.42	1.5	0.5	-0.36	6.4
Total	3.86	1.4	1.3	0.11	5.0

Table 3: Parameters for the axion luminosity from SN entering Eqs. (27) and (28). The coefficients are calculated at a post-bounce time of 1s (see Ref. [41]). The first row refers to the NN bremsstrahlung contribution only [66], ignoring the pion scattering processes and the Δ resonance contribution. The second row gives the total contribution, calculated from the results in Ref. [41]. The mass parameter $\overline{m}$ is defined in Eq. (30).

on a particular combination of C_0 and C_3, and thus only this combination can be constrained. The luminosity can be expressed as [41]

$$L_a = \epsilon_0 \left(\frac{m_N}{f_a}\right)^2 C_{\rm SN}^2 \times 10^{70}\,{\rm erg/s}\,, \tag{27}$$

where ϵ_0 is a numerical factor and

$$C_{\rm SN} = a\Big(C_0^2 + b\,C_3^2 + c\,C_0 C_3\Big)^{1/2}\,. \tag{28}$$

The numerical values of the coefficients ϵ_0, a and b can be found in Table 3. In the table we present, in the first line, the results obtained by considering only the purely NN bremsstrahlung production, which corresponds to the first line of Eq. (1). The results for the total emission rate are given in the second line (we remind to the reader that up until very recently, the NN bremsstrahlung production was the only process considered for estimating SN axion emission rate.)

Notice that, as evident from Table 3, the addition of the pion-induced scatterings increases the relative importance of C_3 (controlled by the coefficients b and c) and thus enhances the effects of the RG corrections. More specifically, from Eq. (28), and assuming $\Delta C_0 \approx 0$, we find

$$\Delta C_{\rm SN} \simeq a^2\Big(b\,C_3 + \frac{c}{2}\,C_0\Big)\frac{\Delta C_3}{C_{\rm SN}}\,. \tag{29}$$

As expected, the RG effects are reduced in the case of purely NN-bremsstrahlung production, due to the partial cancellation between the b and c terms.[11]

Imposing $L_a \leq L_\nu = 3\times 10^{52}$ erg/s [41], we find the bound on the axion mass

$$m_a \leq \frac{\overline{m}}{C_{\rm SN}}\,, \quad \text{with} \quad \overline{m} = \frac{9.9\,{\rm meV}}{\sqrt{\epsilon_0}}\,. \tag{30}$$

In the case of for DFSZ axions, this bound is shown in Fig. 4.

Specializing on the DFSZ axion case, we immediately find from Tab. 1,

$$C_{\rm SN}^{\rm DFSZ} = 0.2\,a\,\sqrt{1 + 2.15\,c\sin^2\beta + 4.5\,b\sin^4\beta}\,. \tag{31}$$

and

$$\left(\frac{\Delta C_{\rm SN}}{C_{\rm SN}}\right)^{\rm DFSZ} = \left[\frac{\Big(0.30\,c + 1.3\,b\sin^2\beta\Big)\cos^2\beta}{1 + 2.15\,c\sin^2\beta + 4.6\,b\sin^4\beta}\right] I(x)\,. \tag{32}$$

Note that the above expression is never larger than about 10%-15%. Thus, for the SN bound RG effects are somewhat less

[11] We should be cautious, however, since this expression is valid only in the limit of $\Delta C_3/C_{\rm SN} \ll 1$ and this condition is not always met. In particular, it is violated at low $\tan\beta$ and high $m_{\rm BSM}$.

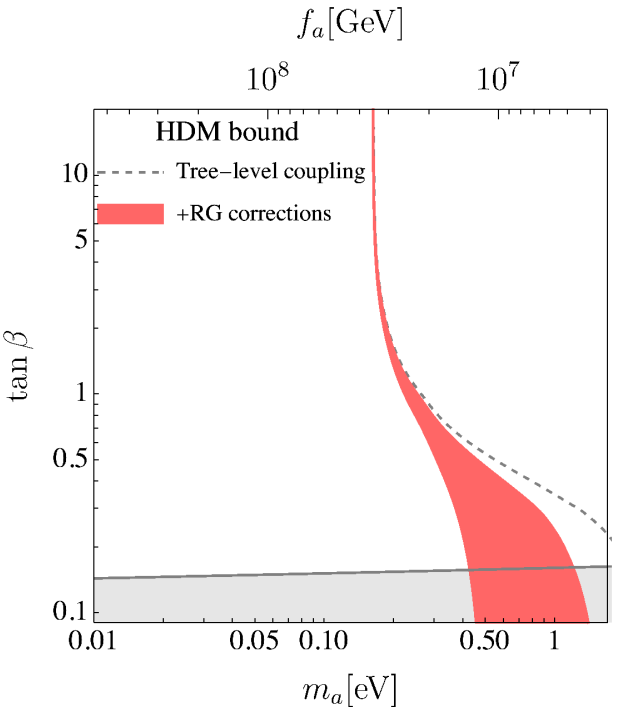


Figure 5: HDM bound in the DFSZ1/2 models. The red region shows the effect of RG corrections, for $m_{\rm BSM}$ ranging from f_a (left border) to 1 TeV (right border). The gray line corresponds to the perturbative unitarity bound on $\tan\beta$ for $m_{\rm BSM} = f_a$.

prominent than in the case of the RGB bound. For comparison, ignoring the contribution from the pion scatterings, gives the combination $C_{\rm SN} \simeq 1.5\sqrt{C_0^2 + 0.50\,C_3^2 - 0.36\,C_0 C_3}$. Notice that, as discussed above, the two results have a significantly different dependence on $C_{0,3}$ and, in particular, the addition of the pion-induced scatterings increases the relative importance of C_3 and thus enhances the dependence on the RG corrections.

3.2. Thermal axion cosmology

If axions are in thermal equilibrium until below the quark-hadron phase transition (which can occur for $m_a \gtrsim 0.1\,$eV) the axion thermal population will give a sizeable contribution to the effective number of extra relativistic degrees of freedom [67], $\Delta N_{\rm eff}$, that is constrained by Big Bang Nucleosynthesis (BBN) [68] and cosmic microwave background (CMB) observations [69, 70]. The highest attainable axion mass from such cosmological constraints is also known as the Hot Dark Matter (HDM) bound. The forecast sensitivity of the planned CMB-S4 [71] and Simons Observatory (SO) [72] surveys will fully cover the mass range in which the axion decouples below or across the QCD crossover, thus a precise determination of the axion-pion thermalization rate, including running effects, would be necessary to set definite targets.[12]

For $T \lesssim T_c$, where $T_c \simeq 155\,$MeV is the QCD deconfinement temperature, the dominant thermalization channels is $a\pi \leftrightarrow \pi\pi$ [13, 49]. It has been recently shown, however, that the standard computation of this process, that is based on chiral perturbation theory (ChPT), breaks down for $T \gtrsim 70$ MeV [50, 52]. Phenomenological extensions of the validity of the chiral expansion, based on unitarization methods, have been proposed in Refs. [51, 52].

In the following, we will consider the unitarized thermal rate based on the Inverse Amplitude Method (IAM), recently discussed in Ref. [52], which gives the thermal scattering rate:

$$\Gamma_a^{\rm IAM}(T) = \left(\frac{C_\pi}{f_a f_\pi}\right)^2 0.150\; T^5 h_{\rm IAM}(m_\pi/T)\,, \qquad (33)$$

with C_π given in Eq. (5) and $m_\pi = 137\,$MeV representing the average neutral/charged pion mass. The numerical function $h_{\rm IAM}$ is provided in Ref. [52] (cf. Fig. 3 of this reference) and is normalized to $h_{\rm IAM}(m_\pi/T_c) = 1$.

We will estimate the impact of RG effects on the HDM bound relying for simplicity on the instantaneous decoupling condition $\Gamma_a(T_D) \simeq H(T_D)$, with $\Gamma_a(T)$ the axion-pion scattering rate given in Eq. (33) and $H(T) = \sqrt{4\pi^3 g_\star(T)/45}\,T^2/m_{\rm pl}$ the Hubble rate, where $m_{\rm pl} = 1.22\times 10^{19}\,$GeV is the Planck mass and $g_\star(T)$ the effective number of relativistic degrees of freedom.[13]

The axion contribution to the effective number of extra relativistic degrees of freedom is given by [67]

$$\Delta N_{\rm eff} \simeq \frac{4}{7}\left(\frac{T_a}{T_\nu}\right)^4 = \frac{4}{7}\left(\frac{43}{4 g_S(T_D)}\right)^{4/3} \simeq 0.027\left(\frac{106.75}{g_S(T_D)}\right)^{4/3}\,, \qquad (34)$$

with T_a/T_ν the ratio of the axion to neutrino temperature at $T \ll 1\,$MeV (i.e. well after ν-decoupling) and $g_S(T_D)$ the number of entropy degrees of freedom at axion decoupling, that in the last relation has been normalised to the total number of SM degrees of freedom $g_S(T > m_t) = 106.75$. We then confront Eq. (34) with the bound on $\Delta N_{\rm eff}$ from Planck's 2018 data [69, 70], and from this we extract a bound on the axion mass.

Our results for the HDM bound in the DFSZ1/2 models are summarised in Fig. 5, where we show the tree-level results compared with the RG corrections included. Again we see that RG effects are especially important at small $\tan\beta$. In Fig. 5 the DFSZ1 and DFSZ2 cases coincide because the (subleading) effects of scattering off leptons have been neglected. In Ref. [75] it was argued that thermalization channels involving axion scattering off leptons can become relevant in DFSZ2 at small $\tan\beta$. However, since RG corrections keep the axion-pion coupling sizeable also in this regime, the effect of lepton scattering becomes accordingly less important.

3.3. Helioscope experiments

One of the most appealing result of the RG correction analysis is the implication for the next generation of experiments

[12] In this paper we will refrain from assessing the impact of CMB-S4 and SO projections on $\Delta N_{\rm eff}$, since these involve an extrapolation of the axion thermalization rate beyond the QCD crossover, which is plagued by large non-perturbative uncertainties [51], and it is still matter of investigation.

[13] For a more refined treatment of the cosmological aspects of axion thermal decoupling see e.g. Refs. [51, 73, 74].

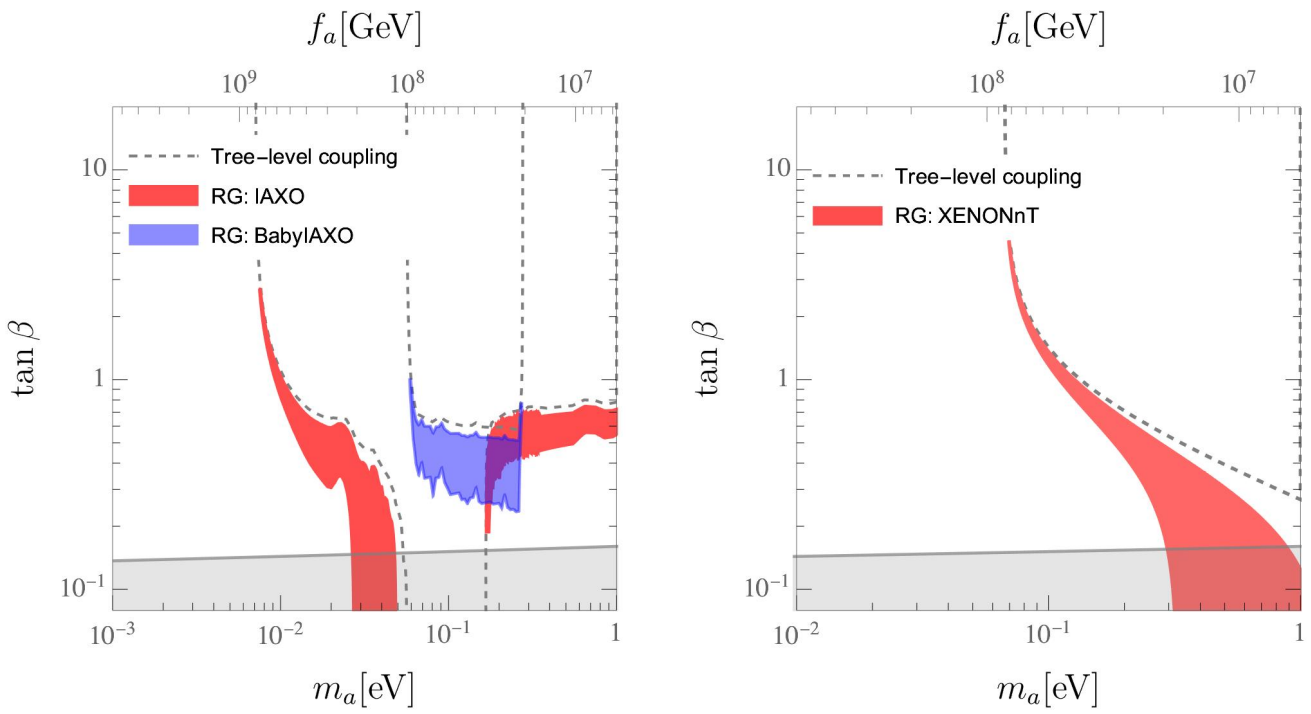


Figure 6: Experimental sensitivity to DFSZ1 axions, including RG effects. *Left Panel*: IAXO and BabyIAXO. *Right Panel*: XENON-nT. In both plots the gray line corresponds to the perturbative unitarity bound on $\tan\beta$ for $m_{\rm BSM} = f_a$.

hunting for solar axions. The main reason is that the solar flux is strongly dependent on the axion-electron coupling and, as we have seen, this can receive large RG corrections. As a consequence, helioscope sensitivities to DFSZ axions, that have been so far estimated using tree level electron-axion couplings, have been underestimated.

Here, we focus mostly on the Sikivie type of axion helioscopes [59]. This kind of experiment is designed to detect solar axions by converting them in X-ray photons using a large laboratory magnetic field. The importance of the axion-electron coupling for Sikivie's helioscope sensitivity to solar axions is expressed by the following relation [9]

$$g_{\gamma 10}^2\left(g_{\gamma 10}^2 + 0.7 g_{e12}^2\right) > \overline{g}_{\gamma 10}^4 \,, \tag{35}$$

where $g_{\gamma 10} = g_{a\gamma}/10^{-10}\text{GeV}^{-1}$, $g_{e12} = g_{ae}/10^{-12}$, and $\overline{g}_{\gamma 10}$ is the helioscope sensitivity to $g_{a\gamma}$ (again, in units of 10^{-10}GeV^{-1}). Notice that $\overline{g}_{a\gamma}$ is, in general, a function of the axion mass. Defining the effective coupling

$$C_{\rm hel} = \left[C_\gamma^2\left(C_\gamma^2 + (37C_e)^2\right)\right]^{1/4} , \tag{36}$$

the above expression leads to the following heliscope sensitivity relation

$$C_{\rm hel} \gtrsim \frac{0.49\,\overline{g}_{\gamma 10}}{(m_a/\text{eV})} \,, \tag{37}$$

which, in the case of the DFSZ axion, can be readily translated into a limit on the $\tan\beta$ accessible to the helioscope as a function of the axion mass. Notice that, according to this expression, the DFSZ sensitivity to $\tan\beta$ (which enters only through C_e), should disappear for $C_\gamma \gg 37C_e$, which is fulfilled for $\tan\beta \ll 0.25$. In general, if the helioscope sensitivity is good enough, there could be mass regions where the entire range of $\tan\beta$ is accessible.

To give an example of an application of Eq. (37), let us consider the case of BabyIAXO, a next-generation axion helioscope presently under construction [76]. Its sensitivity at $m_a = 0.1\,\text{eV}$ is expected to reach $\overline{g}_{\gamma 10} = 0.33$. Using this value and $C_\gamma = 8/3 - 1.92$ for the DFSZ1 model, if RG effects are ignored, one would conclude that at this mass value BabyIAXO could be sensitive to the region $\tan\beta \gtrsim 0.62$. The results of our complete numerical analysis for all values of the axion mass are plotted in the left panel in Fig. 6, where the dashed line contours correspond to the estimated BabyIAXO sensitivity if RG effects are ignored. The reach of the more advanced helioscope experiment IAXO [77] is also shown in the left panel in Fig. 6. In this case we see that there is a mass region for which the experiment is sensitive to all values of $\tan\beta$. When RG corrections are ignored, this region extends to masses between ~ 50 meV and ~ 200 meV. The reason of this is that IAXO is sensitive enough to see the solar axion flux even in models in which axions are only coupled to the photon and not to the electron.

Let us now consider the effects of RG corrections on the projected sensitivities. As shown in Tab. 2, the RG corrections to the effective helioscope coupling is

$$\frac{\Delta C_{\rm hel}}{C_{\rm hel}} = \frac{1}{2}\frac{\Delta C_e/C_e}{1 + \left(C_\gamma/(37C_e)\right)^2} \,, \tag{38}$$

which is valid in the limit of $\Delta C_e/C_e \ll 1$. This condition is always verified in DFSZ2, while for DFSZ1 it holds for

$\tan\beta \gg 0.5\, l(x)^{1/2}$ (Cf. Tab. 1). Since in the case of BabyIAXO the expected sensitivity is not sufficient to detect DFSZ axions unless $\tan\beta \gtrsim 0.6$ (see Fig. 6) which implies $C_\gamma/(37C_e) \ll 1$, we can simplify the correction to the effective coupling to

$$\left(\frac{\Delta C_{\rm hel}}{C_{\rm hel}}\right)^{\rm BabyIAXO} \simeq \frac{\Delta C_e}{2C_e}\,, \tag{39}$$

which can be readily estimated using our results from the Tab 1. Notice that this correction can be quite sizable and implies that the reach of BabyIAXO to small electron couplings (low $\tan\beta$ values) can be pushed down significantly, as is shown by the blue region in the left panel of Fig. 6.

The impact of RG corrections on the IAXO sensitivity to DFSZ1 axions is also shown in the left panel of Fig. 6, and corresponds to the red regions. In this case we notice an interesting effect, that is that the IAXO reach in the region of small $\tan\beta$ is sizeably enlarged for all values of $m_{\rm BSM}$, since the solar axion flux is necessarily larger than what predicted ignoring the RG corrections. As a result, the mass region for which IAXO is sensitive to the entire range of $\tan\beta$ is extended.

Finally, the correction to the axion-electron coupling has also an obvious impact on experiments which detect axions through the axio-electric effect. Such experiments include large underground detectors such as Panda-X [57], LUX [56], or XENON-nT [58], originally designed for dark matter searches. The RG modification of the axion-electron coupling extends the potential of these experiments to explore the DFSZ parameter space. Our numerical results in the case of XENON-nT are shown in the right panel of Fig. 6. A fundamental difference with respect to the previous results is that, because of the RG-induced corrections, in principle XENON-nT could be sensitive to DFSZ1 axions for any value of $\tan\beta$. However, the current experimental sensitivity is insufficient to reach inside the mass region allowed by the RGB bound discussed in Sect. 3.1 (see the left panel in Fig. 4).

4. Conclusions

In this paper, we have studied the impact of RG effects on QCD axion phenomenology, focusing on DFSZ models. We have shown that running effects on axion couplings depend crucially on the scale at which the heavy Higgs states are integrated out, and the 2HDM effectively reduces to the SM with a single light Higgs. We have discussed the implications of running axion couplings on astrophysical and cosmological bounds, as well as the sensitivity of helioscope experiments such as (Baby)IAXO. We have found that running effects are sizable even in the most conservative case in which the 2HDM structure keeps holding down to the TeV-scale, and thus they can never be neglected. We have also provided simple analytic expressions fitted to reproduce the numerical solutions of the RG equations, which can be a useful tool for studying the implications of running axion couplings. In the case of an axion discovery, running effects might prove to be crucial in order to reconstruct the axion UV completion.

Acknowledgments

We thank Kiwoon Choi and Giovanni Villadoro for useful discussions. The work of L.D.L. is funded by the European Union – NextGenerationEU and by the University of Padua under the 2021 STARS Grants@Unipd programme (Acronym and title of the project: CPV-Axion – Discovering the CP-violating axion) and by the INFN Iniziative Specifica APINE. The work of L.D.L. and G.P. is supported by the European Union's Horizon 2020 research and innovation programme under the Marie Skłodowska-Curie grant agreement No 860881-HIDDEN. The work of E.N. was supported by the Estonian Research Council grant PRG1884 and by the INFN "Iniziativa Specifica" Theoretical Astroparticle Physics (TAsP-LNF). S.O. and F.M. acknowledge financial support from a Maria Zambrano fellowship and the State Agency for Research of the Spanish Ministry of Science and Innovation through the Unit of Excellence María de Maeztu 2020-2023 award to the Institute of Cosmos Sciences (CEX2019-000918-M) and from PID2019-105614GB-C21, 2017-SGR-929 and 2021-SGR-249 grants. This article is based upon work from COST Action COSMIC WISPers CA21106, supported by COST (European Cooperation in Science and Technology). M.G. research was partially supported by funds from "European Union NextGenerationEU/PRTR" (Planes complementarios, Programa de Astrofísica y Física de Altas EnergÃas) and from the European Union's Horizon 2020 research and innovation programme under the European Research Council (ERC) grant agreement ERC-2017-AdG788781 (IAXO+). We thank the Galileo Galilei Institute for Theoretical Physics for hospitality during the completion of this work.

Appendix A. RG equations for DFSZ axion couplings

In order to take into account running effects it is convenient to adopt the Georgi-Kaplan-Randall (GKR) field basis [78], where the PQ symmetry is realised non-linearly, so that under a $\mathrm{U}(1)_{\rm PQ}$ symmetry transformation all fields are invariant except for the axion field, which changes by an additive constant $a \to a + \alpha f$, that is

$$\begin{aligned}\mathcal{L}_a^{\rm GKR-2HDM} &= \frac{1}{2}\partial_\mu a \partial^\mu a + \sum_{A=G,W,B} c_A \frac{g_A^2}{32\pi^2}\frac{a}{f}F^A\tilde{F}^A \\ &+ \frac{\partial_\mu a}{f}\Big[c_{H_u} H_u^\dagger i\overleftrightarrow{D^\mu} H_u + c_{H_d} H_d^\dagger i\overleftrightarrow{D^\mu} H_d + \bar{q}_L c_{q_L}\gamma^\mu q_L \\ &+ \bar{u}_R c_{u_R}\gamma^\mu u_R + \bar{d}_R c_{d_R}\gamma^\mu d_R + \bar{\ell}_L c_{\ell_L}\gamma^\mu \ell_L + \bar{e}_R c_{e_R}\gamma^\mu e_R\Big]\,,\end{aligned} \tag{A.1}$$

where $H_{u,d}^\dagger \overleftrightarrow{D^\mu} H_{u,d} \equiv H_{u,d}^\dagger (D^\mu H_{u,d}) - (D^\mu H_{u,d})^\dagger H_{u,d}$ and $c_{q_L}, \ldots$ are diagonal matrices in generation space. Note that in the effective field theory below f we have neglected the heavy $O(f)$ radial mode of Φ and we focused for simplicity on the 2HDM. In order to match an explicit axion model to the effective Lagrangian in Eq. (A.1) at the high scale $\mu \sim O(f)$, we perform an axion dependent field redenfinition: $\psi \to e^{-i\mathcal{X}_\psi a/f}\psi$, where ψ spans over all the fields, and $\mathcal{X}_\psi$ is the corresponding PQ charge. Due to $\mathrm{U}(1)_{\rm PQ}$ symmetry, the non-derivative part of the renormalizable Lagrangian is invariant upon this field redefinition,

while the $d = 5$ operators in Eq. (A.1) are generated from the variation of the kinetic terms and from the chiral anomaly. The couplings are then identified as

$$c_\psi = \mathcal{X}_\psi\,, \tag{A.2}$$

$$c_A = \sum_{\psi_R} 2\mathcal{X}_{\psi_R} \mathrm{Tr}\, T_A^2(\psi_R) - \sum_{\psi_L} 2\mathcal{X}_{\psi_L} \mathrm{Tr}\, T_A^2(\psi_L)\,, \tag{A.3}$$

where in the second equation $c_{\psi_{R,L}}$ refer to the charges of the chiral fermion fields.[14] For the DFSZ1 model introduced in Sect. 2.2, with e.g. the operator $H_u H_d \Phi^\dagger$ in the scalar potential, the universal charges $\mathcal{X}_\psi$ can be set to

$$\mathcal{X}_q = \mathcal{X}_\ell = 0\,,\ \mathcal{X}_u = -\mathcal{X}_{H_u}\,,\ \mathcal{X}_d = -\mathcal{X}_{H_d}\,,\ \mathcal{X}_e = -\mathcal{X}_{H_d}\,, \tag{A.4}$$

where $\mathcal{X}_{H_u} = c_\beta^2$ and $\mathcal{X}_{H_d} = s_\beta^2$. The DFSZ2 model features a similar charge assignment, with instead $\mathcal{X}_e = \mathcal{X}_{H_u}$. For the anomaly coefficients in Eq. (A.3) in the case of the DFSZ1 model one has $(c_G, c_W, c_B) = (-3, 0, -8)$ and, in particular, the electromagnetic to QCD anomaly ratio is $E/N \equiv (c_W + c_B)/c_G = 8/3$. Similarly, for the DFSZ2 model one finds $(c_G, c_W, c_B) = (-3, 0, -2)$ and $E/N = 2/3$.

Running effects induced by Yukawa couplings (and in particular by the top Yukawa which is the most relevant one) only occur below the scale of the heavy radial modes of the 2HDM, denoted as $m_{\rm BSM} \simeq m_{H,A,H^\pm}$, with the heavy scalars assumed to be degenerate in the decoupling limit (see e.g. [34]). This is due to the fact that as long as the complete set of Higgs doublets appear in the effective field theory, the PQ current is conserved (up to anomalous effects) and thus the couplings, which correspond to PQ charges, do not renormalize. Once the heavy scalar components are integrated out, the sum-rule of PQ charges set by $\mathrm{U}(1)_{\rm PQ}$ invariance breaks down, and non-vanishing contributions to the running of the couplings arise (see e.g. [14]). We can now directly match Eq. (A.1) at the scale $\mu = O(m_{\rm BSM})$ with a GKR basis featuring only one SM-like Higgs doublet

$$\begin{aligned}\mathcal{L}_a^{\rm GKR-SM} &= \frac{1}{2}\partial_\mu a \partial^\mu a + \sum_{A=G,W,B} c_A \frac{g_A^2}{32\pi^2}\frac{a}{f} F^A \tilde{F}^A \\ &+ \frac{\partial_\mu a}{f}\Big[c_H H^\dagger i\overleftrightarrow{D^\mu} H + \bar{q}_L c_{q_L}\gamma^\mu q_L \\ &+ \bar{u}_R c_{u_R}\gamma^\mu u_R + \bar{d}_R c_{d_R}\gamma^\mu d_R + \bar{\ell}_L c_{\ell_L}\gamma^\mu \ell_L + \bar{e}_R c_{e_R}\gamma^\mu e_R\Big]\,,\end{aligned} \tag{A.5}$$

where $c_H = c_{H_u} s_\beta^2 - c_{H_d} c_\beta^2$, which follows from the projections on the SM Higgs doublet $H \sim (1, 2, -1/2)$: $H_u \to s_\beta H$ and $H_d \to c_\beta \tilde{H}$, consistently with the definition of $\tan\beta = v_u/v_d$. In particular, by employing global $\mathrm{U}(1)_Y$ invariance, it is convenient to cast the RG equations in a form that does not depend explicitly on c_H. This can be achieved via the axion-dependent field redefinition: $\psi \to \psi' = e^{-ic_H\beta_\psi a/f}\psi$, with $\beta_\psi = Y_\psi/Y_H$ the ratio of the corresponding hypercharges, which redefines the effective couplings as $c'_\psi = c_\psi - c_H\beta_\psi$ (so in particular $c'_H = 0$).

[14] Note that our anomaly coefficients c_A have opposite sign with respect to those in Refs. [14, 15, 17]. This is due to the fact that we are using a different convention for the Levi-Civita tensor, namely $\epsilon^{0123} = -1$.

In this basis the RG equations read:

$$\begin{aligned}(4\pi)^2\frac{dc'_{q_L}}{d\log\mu} &= \frac{1}{2}\{c'_{q_L}, Y_u Y_u^\dagger + Y_d Y_d^\dagger\} - Y_u c'_{u_R} Y_u^\dagger - Y_d c'_{d_R} Y_d^\dagger \\ &+ \left(8\alpha_s^2\widetilde{c}_G + \frac{9}{2}\alpha_2^2\widetilde{c}_W + \frac{1}{6}\alpha_1^2\widetilde{c}_B\right)\mathbf{1} - \beta_q\,\gamma_H\,\mathbf{1}\,, \\ (4\pi)^2\frac{dc'_{u_R}}{d\log\mu} &= \{c'_{u_R}, Y_u^\dagger Y_u\} - 2Y_u^\dagger c'_{q_L} Y_u - \left(8\alpha_s^2\widetilde{c}_G + \frac{8}{3}\alpha_1^2\widetilde{c}_B\right)\mathbf{1} \\ &- \beta_u\,\gamma_H\,\mathbf{1}\,, \\ (4\pi)^2\frac{dc'_{d_R}}{d\log\mu} &= \{c'_{d_R}, Y_d^\dagger Y_d\} - 2Y_d^\dagger c'_{q_L} Y_d - \left(8\alpha_s^2\widetilde{c}_G + \frac{2}{3}\alpha_1^2\widetilde{c}_B\right)\mathbf{1} \\ &- \beta_d\,\gamma_H\,\mathbf{1}\,, \\ (4\pi)^2\frac{dc'_{\ell_L}}{d\log\mu} &= \frac{1}{2}\{c'_{\ell_L}, Y_e Y_e^\dagger\} - Y_e c'_{e_R} Y_e^\dagger + \left(\frac{9}{2}\alpha_2^2\widetilde{c}_W + \frac{3}{2}\alpha_1^2\widetilde{c}_B\right)\mathbf{1} \\ &- \beta_\ell\,\gamma_H\,\mathbf{1}\,, \\ (4\pi)^2\frac{dc'_{e_R}}{d\log\mu} &= \{c'_{e_R}, Y_e^\dagger Y_e\} - 2Y_e^\dagger c'_{\ell_L} Y_e - 6\alpha_1^2\widetilde{c}_B\,\mathbf{1} - \beta_e\,\gamma_H\,\mathbf{1}\,,\end{aligned} \tag{A.6}$$

where

$$\begin{aligned}\gamma_H &= -2\,\mathrm{Tr}\left(3Y_u^\dagger c'_{q_L} Y_u - 3Y_d^\dagger c'_{q_L} Y_d - Y_e^\dagger c'_{\ell_L} Y_e\right) \\ &+ 2\,\mathrm{Tr}\left(3Y_u c'_{u_R} Y_u^\dagger - 3Y_d c'_{d_R} Y_d^\dagger - Y_e c'_{e_R} Y_e^\dagger\right), \\ \widetilde{c}_G &= c_G - \mathrm{Tr}\left(c'_{u_R} + c'_{d_R} - 2c'_{q_L}\right), \\ \widetilde{c}_W &= c_W + \mathrm{Tr}\left(3c'_{q_L} + c'_{\ell_L}\right), \\ \widetilde{c}_B &= c_B - \mathrm{Tr}\left(\frac{1}{3}(8c'_{u_R} + 2c'_{d_R} - c'_{q_L}) + 2c'_{e_R} - c'_{\ell_L}\right).\end{aligned} \tag{A.7}$$

Note that the c_A ($A = G, W, B$) Wilson coefficients in Eq. (A.7) do not run at one loop, since in the normalization of Eq. (A.1) the scale dependence of the operator $aF^A\tilde{F}^A$ is accounted for by the running of the gauge couplings [17, 79].

Eq. (A.5) is matched at the scale $\mu = O(m_Z)$ with the $\mathrm{SU}(3)_C \times \mathrm{U}(1)_{\rm EM}$-invariant axion effective Lagrangian below the electroweak scale

$$\mathcal{L}_a \supset \mathcal{L}_{GF} + \mathcal{L}_f\,, \tag{A.8}$$

$$\mathcal{L}_{GF} = \frac{g_s^2}{32\pi^2}\frac{a}{f_a} G\tilde{G} + \frac{c_\gamma}{c_G}\frac{e^2}{32\pi^2}\frac{a}{f_a} F\tilde{F}\,, \tag{A.9}$$

$$\mathcal{L}_f = \sum_{f=u,d,e}\frac{\partial_\mu a}{2f_a}\bar{f}_i\gamma^\mu\Big[(C_f^V)_{ij} + (C_f^A)_{ij}\gamma_5\Big]f_j\,, \tag{A.10}$$

where we have introduced the standard QCD normalization factor for the $aG\tilde{G}$ term and defined the axion decay constant $f_a = f/c_G$, while $c_\gamma = c_W + c_B$. We further have

$$C_f^V = \frac{1}{c_G}(U_{f_R} c'_{f_R} U_{f_R}^\dagger + U_{f_L} c'_{f_L} U_{f_L}^\dagger)\,, \tag{A.11}$$

$$C_f^A = \frac{1}{c_G}(U_{f_R} c'_{f_R} U_{f_R}^\dagger - U_{f_L} c'_{f_L} U_{f_L}^\dagger)\,, \tag{A.12}$$

where $U_{f_{L,R}}$ are the unitary matrices that diagonalize the SM fermion mass matrices, and $c'_{u_L} = c'_{d_L} = c'_{q_L}$. Note that the diagonal vector couplings $(C_f^V)_{ii}$ can be always set to zero thanks

to the conservation of the vector current. In our case, since the models that we have considered enjoy flavour universality, the matrices of couplings $c'_{f_{R,L}}$ are proportional to the identity, then $\mathcal{L}_f$ simplifies to:

$$\mathcal{L}_f = \sum_{f=u,d,e} C_f^A \frac{\partial_\mu a}{2f_a} \bar{f}\gamma^\mu\gamma_5 f\,, \tag{A.13}$$

$$C_f^A = \frac{1}{c_G}(c'_{f_R} - c'_{f_L})\,. \tag{A.14}$$

After including matching corrections at the weak scale [17], the running for $\mu < m_Z$ is given by

$$\begin{aligned}
(4\pi)^2 \frac{dC_u^A}{d\log\mu} &= -16\alpha_s^2\widetilde{c}_G - \frac{8}{3}\alpha_{\rm em}^2\widetilde{c}_\gamma\,,\\
(4\pi)^2 \frac{dC_d^A}{d\log\mu} &= -16\alpha_s^2\widetilde{c}_G - \frac{2}{3}\alpha_{\rm em}^2\widetilde{c}_\gamma\,,\\
(4\pi)^2 \frac{dC_e^A}{d\log\mu} &= -6\alpha_{\rm em}^2\widetilde{c}_\gamma\,,
\end{aligned} \tag{A.15}$$

with

$$\widetilde{c}_G(\mu) = 1 - \sum_q C_q^A(\mu)\Theta(\mu - m_q)\,, \tag{A.16}$$

$$\widetilde{c}_\gamma(\mu) = \frac{c_\gamma}{c_G} - 2\sum_f N_c^f Q_f^2 C_f^A(\mu)\Theta(\mu - m_f)\,, \tag{A.17}$$

where $\Theta(x)$ is the Heaviside theta function, while N_c^f and Q_f denote respectively the colour number and EM charge of the fermion f.

The axion-nucleon couplings, neglecting the tiny contributions of the matrix elements $\Delta_{t,b,c}$ of the heavy flavours, can be calculated by using Eqs. (3)-(4), with $C_{u,d,s} = C^A_{u,d,s}(2\,\text{GeV})$ evaluated by numerically solving the RG equations, Eqs. (A.6) and (A.15), starting from the boundary conditions set at the scale f (cf. below Eq. (A.3)).

Appendix B. Numerical fit to RG effects

Running of axion couplings is examined in detail in Refs. [14, 15, 17, 80], where a complete set of one-loop (and partially two-loop) anomalous dimensions are derived including matching corrections at the EW scale [17]. The leading contribution to the running axion couplings arises from top loop diagrams induced by the axion-top coupling C_t. The RG evolved couplings at $\mu = 2\,\text{GeV}$ are thus expressed to a good approximation by

$$C_\Psi(2\,\text{GeV}) \simeq C_\Psi(f_a) + r_\Psi^t(m_{\rm BSM})\, C_t(f_a), \tag{B.1}$$

where $\Psi = u, d, e$. Note that the running occurs below the heavy Higgs scale $m_{\rm BSM} \simeq m_{H,A,H^+}$, where in the decoupling limit the heavy scalars are assumed to be approximately degenerate, and $r_\Psi^t(m_{\rm BSM})$ is a function only of $m_{\rm BSM}$.

Keeping only the top Yukawa and the strong gauge couplings, the running of C_Ψ below $\mu = m_{\rm BSM}$ is governed by [14, 15, 17, 80]

$$\frac{dC_\Psi}{d\ln\mu} \simeq -T_{3,\Psi}\frac{3Y_t^2}{4\pi^2}\, C_t\,\Theta(\mu - \mu_w) - a_\Psi\frac{\alpha_s^2}{\pi^2}\widetilde{c}_G\,, \tag{B.2}$$

where $T_{3,\Psi}$ is the weak isospin of Ψ, $a_\Psi = 1$ for quarks and 0 for leptons, $\mu_w = O(m_Z)$ is a matching scale at which weak gauge bosons, Higgs boson and top quark are integrated out, with $\widetilde{c}_G$ defined in Eq. (A.16).

We see from Eq. (B.2) that the RG corrections to the axion couplings consist of one-loop iso-vector contribution, proportional to the weak isospin $T_{3,\Psi}$, and a two-loop level iso-scalar contribution generated from $\widetilde{c}_G$,[15] and can be expressed in the form

$$r_\Psi^t(m_{\rm BSM}) \simeq T_{3,\Psi}\, r_3^t(m_{\rm BSM}) + \frac{a_\Psi}{2}\, r_0^t(m_{\rm BSM})\,, \tag{B.3}$$

which, for the running of $C_{3,0}$, yields

$$r_3^t \simeq r_u^t - r_d^t \simeq -2r_e^t\,, \tag{B.4}$$

$$r_0^t \simeq r_u^t + r_d^t\,. \tag{B.5}$$

Note that $r_{3,0}^t$ are independent of Ψ to a good precision, even after including the threshold corrections at the EW scale, which turn out to be iso-vector (numerically $\left|(r_0^t)_{\rm th}/(r_3^t)_{\rm th}\right| \sim 10^{-6}$).

Let us now derive approximate formulae for $r_{3,0}^t(m_{\rm BSM})$. To this end, we first evaluate the running effects by numerically solving the full set of the RG equations including the threshold corrections at the EW scale [17]. In the calculation the two-loop running for the SM gauge and Yukawa couplings is implemented, with their input values at $\mu_w = m_Z$ taken from Ref. [38]. A set of numerical values for $r_{3,0}^t(m_{\rm BSM})$ are tabulated in Tab. B.4. These values are accurately fitted by the following fitting functions:

$$r_3^t(m_{\rm BSM}) \simeq r_u^t - r_d^t \simeq -0.54\ln\left(\sqrt{x} - 0.52\right), \tag{B.6}$$

$$r_0^t(m_{\rm BSM}) \simeq r_u^t + r_d^t \simeq 3.8\times10^{-4}\ln^2(x - 1.25)\,, \tag{B.7}$$

with $x = \log_{10}(m_{\rm BSM}/\,\text{GeV})$. Eq. (B.6) agrees with the numerical results within 2% accuracy in the $1\,\text{TeV} \le m_{\rm BSM} \le 10^{18}\,\text{GeV}$ range. The precision of Eq. (B.7) is better than 6%. However, since $|r_0^t/r_3^t| \lesssim 0.5\%$, this function does not affect numerically r_Ψ^t.

References

[1] R. D. Peccei and H. R. Quinn, "CP Conservation in the Presence of Instantons," *Phys. Rev. Lett.* **38** (1977) 1440–1443.

[2] R. D. Peccei and H. R. Quinn, "Constraints Imposed by CP Conservation in the Presence of Instantons," *Phys. Rev.* **D16** (1977) 1791–1797.

[3] S. Weinberg, "A New Light Boson?," *Phys. Rev. Lett.* **40** (1978) 223–226.

[4] F. Wilczek, "Problem of Strong p and t Invariance in the Presence of Instantons," *Phys. Rev. Lett.* **40** (1978) 279–282.

[5] J. E. Kim, "Weak Interaction Singlet and Strong CP Invariance," *Phys. Rev. Lett.* **43** (1979) 103.

[6] M. A. Shifman, A. I. Vainshtein, and V. I. Zakharov, "Can Confinement Ensure Natural CP Invariance of Strong Interactions?," *Nucl. Phys.* **B166** (1980) 493.

[15] In the DFSZ models, $\widetilde{c}_G = 0$ at $\mu = m_{\rm BSM}$ and it develops a nonzero value because of the running of C_q. This means that the running effects from $\widetilde{c}_G$ are also proportional to $C_t(f_a)$, allowing to parametrise this iso-scalar contribution in the form of Eq. (B.1).

$m_{\rm BSM}$ [GeV]	r_u^t	r_d^t	r_e^t	$r_3^t = r_u^t - r_d^t$	$r_0^t = r_u^t + r_d^t$
10^3	−0.0523595	0.0524821	0.0524214	−0.104842	0.000122546
10^4	−0.104883	0.105251	0.105072	−0.210134	0.000368801
10^5	−0.145433	0.146074	0.145764	−0.291507	0.000640706
10^6	−0.177998	0.178907	0.178469	−0.356906	0.000909250
10^7	−0.204893	0.206057	0.205498	−0.410949	0.00116422
10^8	−0.227574	0.228976	0.228305	−0.456550	0.00140241
10^9	−0.247016	0.248639	0.247865	−0.495655	0.00162345
10^{10}	−0.263900	0.265729	0.264859	−0.529629	0.00182809
10^{11}	−0.278732	0.280749	0.279793	−0.559481	0.00201769
10^{12}	−0.291859	0.294052	0.293015	−0.585911	0.00219320
10^{13}	−0.303574	0.305930	0.304819	−0.609504	0.00235605
10^{14}	−0.314096	0.316603	0.315424	−0.630699	0.00250738
10^{15}	−0.323599	0.326247	0.325006	−0.649847	0.00264829
10^{16}	−0.332225	0.335005	0.333705	−0.667230	0.00277971
10^{17}	−0.340088	0.342991	0.341637	−0.683079	0.00290251
10^{18}	−0.347283	0.350300	0.348897	−0.697583	0.00301745

Table B.4: The numerical values of $r_\Psi^t(m_{\rm BSM})$ and $r_{3,0}^t(m_{\rm BSM})$, which are obtained by numerically solving the full RGEs, with the threshold corrections at the EW scale included.

[7] A. R. Zhitnitsky, "On Possible Suppression of the Axion Hadron Interactions. (In Russian)," *Sov. J. Nucl. Phys.* **31** (1980) 260. [Yad. Fiz.31,497(1980)].

[8] M. Dine, W. Fischler, and M. Srednicki, "A Simple Solution to the Strong CP Problem with a Harmless Axion," *Phys. Lett.* **B104** (1981) 199–202.

[9] L. Di Luzio, M. Giannotti, E. Nardi, and L. Visinelli, "The landscape of QCD axion models," *Phys. Rept.* **870** (2020) 1–117, arXiv:2003.01100 [hep-ph].

[10] I. G. Irastorza and J. Redondo, "New experimental approaches in the search for axion-like particles," *Prog. Part. Nucl. Phys.* **102** (2018) 89–159, arXiv:1801.08127 [hep-ph].

[11] P. Sikivie, "Invisible Axion Search Methods," arXiv:2003.02206 [hep-ph].

[12] M. Srednicki, "Axion Couplings to Matter. 1. CP Conserving Parts," *Nucl. Phys. B* **260** (1985) 689–700.

[13] S. Chang and K. Choi, "Hadronic axion window and the big bang nucleosynthesis," *Phys. Lett. B* **316** (1993) 51–56, arXiv:hep-ph/9306216.

[14] K. Choi, S. H. Im, H. J. Kim, and H. Seong, "Precision axion physics with running axion couplings," *JHEP* **08** (2021) 058, arXiv:2106.05816 [hep-ph].

[15] K. Choi, S. H. Im, C. B. Park, and S. Yun, "Minimal Flavor Violation with Axion-like Particles," *JHEP* **11** (2017) 070, arXiv:1708.00021 [hep-ph].

[16] M. Chala, G. Guedes, M. Ramos, and J. Santiago, "Running in the ALPs," *Eur. Phys. J. C* **81** no. 2, (2021) 181, arXiv:2012.09017 [hep-ph].

[17] M. Bauer, M. Neubert, S. Renner, M. Schnubel, and A. Thamm, "The Low-Energy Effective Theory of Axions and ALPs," *JHEP* **04** (2021) 063, arXiv:2012.12272 [hep-ph].

[18] J. Bonilla, I. Brivio, M. B. Gavela, and V. Sanz, "One-loop corrections to ALP couplings," *JHEP* **11** (2021) 168, arXiv:2107.11392 [hep-ph].

[19] L. Di Luzio, F. Mescia, E. Nardi, P. Panci, and R. Ziegler, "Astrophobic Axions," *Phys. Rev. Lett.* **120** no. 26, (2018) 261803, arXiv:1712.04940 [hep-ph].

[20] F. Bjorkeroth, L. Di Luzio, F. Mescia, E. Nardi, P. Panci, and R. Ziegler, "Axion-electron decoupling in nucleophobic axion models," *Phys. Rev. D* **101** no. 3, (2020) 035027, arXiv:1907.06575 [hep-ph].

[21] L. Di Luzio, F. Mescia, E. Nardi, and S. Okawa, "Renormalization group effects in astrophobic axion models," *Phys. Rev. D* **106** no. 5, (2022) 055016, arXiv:2205.15326 [hep-ph].

[22] G. C. Branco, P. M. Ferreira, L. Lavoura, M. N. Rebelo, M. Sher, and J. P. Silva, "Theory and phenomenology of two-Higgs-doublet models," *Phys. Rept.* **516** (2012) 1–102, arXiv:1106.0034 [hep-ph].

[23] M. Krause, R. Lorenz, M. Muhlleitner, R. Santos, and H. Ziesche, "Gauge-independent Renormalization of the 2-Higgs-Doublet Model," *JHEP* **09** (2016) 143, arXiv:1605.04853 [hep-ph].

[24] **Particle Data Group** Collaboration, P. A. Zyla *et al.*, "Review of Particle Physics," *PTEP* **2020** no. 8, (2020) 083C01.

[25] L. Di Luzio, F. Mescia, and E. Nardi, "Redefining the Axion Window," *Phys. Rev. Lett.* **118** no. 3, (2017) 031801, arXiv:1610.07593 [hep-ph].

[26] L. Di Luzio, F. Mescia, and E. Nardi, "Window for preferred axion models," *Phys. Rev.* **D96** no. 7, (2017) 075003, arXiv:1705.05370 [hep-ph].

[27] M. Bauer, M. Neubert, and A. Thamm, "Collider Probes of Axion-Like Particles," *JHEP* **12** (2017) 044, arXiv:1708.00443 [hep-ph].

[28] G. Grilli di Cortona, E. Hardy, J. Pardo Vega, and G. Villadoro, "The QCD axion, precisely," *JHEP* **01** (2016) 034, arXiv:1511.02867 [hep-ph].

[29] K. Choi, H. J. Kim, H. Seong, and C. S. Shin, "Axion emission from supernova with axion-pion-nucleon contact interaction," *JHEP* **02** (2022) 143, arXiv:2110.01972 [hep-ph].

[30] S.-Y. Ho, J. Kim, P. Ko, and J.-h. Park, "Supernova axion emissivity with $\Delta(1232)$ resonance in heavy baryon chiral perturbation theory," *Phys. Rev. D* **107** no. 7, (2023) 075002, arXiv:2212.01155 [hep-ph].

[31] **Flavour Lattice Averaging Group (FLAG Review 2023 update)** Collaboration. HTTP://FLAG.UNIBE.CH/2021/.

[32] J. Liang, Y.-B. Yang, T. Draper, M. Gong, and K.-F. Liu, "Quark spins and Anomalous Ward Identity," *Phys. Rev. D* **98** no. 7, (2018) 074505, arXiv:1806.08366 [hep-ph].

[33] **Flavour Lattice Averaging Group (FLAG)** Collaboration, Y. Aoki *et al.*, "FLAG Review 2021," *Eur. Phys. J. C* **82** no. 10, (2022) 869, arXiv:2111.09849 [hep-lat].

[34] J. F. Gunion and H. E. Haber, "The CP conserving two Higgs doublet model: The Approach to the decoupling limit," *Phys. Rev. D* **67** (2003) 075019, arXiv:hep-ph/0207010.

[35] S. Bertolini, L. Di Luzio, H. Kolešová, and M. Malinský, "Massive neutrinos and invisible axion minimally connected," *Phys. Rev. D* **91** no. 5, (2015) 055014, arXiv:1412.7105 [hep-ph].

[36] D. Espriu, F. Mescia, and A. Renau, "Axion-Higgs interplay in the two Higgs-doublet model," *Phys. Rev. D* **92** no. 9, (2015) 095013, arXiv:1503.02953 [hep-ph].

[37] L. Di Luzio, J. F. Kamenik, and M. Nardecchia, "Implications of perturbative unitarity for scalar di-boson resonance searches at LHC," *Eur. Phys. J. C* **77** no. 1, (2017) 30, arXiv:1604.05746 [hep-ph].

[38] S. Antusch and V. Maurer, "Running quark and lepton parameters at various scales," *JHEP* **11** (2013) 115, arXiv:1306.6879 [hep-ph].

[39] P. Carenza, B. Fore, M. Giannotti, A. Mirizzi, and S. Reddy, "Enhanced Supernova Axion Emission and its Implications," *Phys. Rev. Lett.* **126** no. 7, (2021) 071102, arXiv:2010.02943 [hep-ph].

[40] T. Fischer, P. Carenza, B. Fore, M. Giannotti, A. Mirizzi, and S. Reddy, "Observable signatures of enhanced axion emission from protoneutron stars," *Phys. Rev. D* **104** no. 10, (2021) 103012, arXiv:2108.13726 [hep-ph].

[41] A. Lella, P. Carenza, G. Lucente, M. Giannotti, and A. Mirizzi, "Proto-neutron stars as cosmic factories for massive axion-like-particles," arXiv:2211.13760 [hep-ph].

[42] G. Raffelt and L. Stodolsky, "New Particles From Nuclear Reactions in the Sun," *Phys. Lett. B* **119** (1982) 323.

[43] **CAST** Collaboration, S. Andriamonje *et al.*, "Search for 14.4-keV solar axions emitted in the M1-transition of Fe-57 nuclei with CAST," *JCAP* **12** (2009) 002, arXiv:0906.4488 [hep-ex].

[44] **Borexino** Collaboration, G. Bellini *et al.*, "Search for Solar Axions Produced in $p(d,{}^3\mathrm{He})$A Reaction with Borexino Detector," *Phys. Rev. D* **85** (2012) 092003, arXiv:1203.6258 [hep-ex].

[45] A. Bhusal, N. Houston, and T. Li, "Searching for Solar Axions Using Data from the Sudbury Neutrino Observatory," *Phys. Rev. Lett.* **126** no. 9, (2021) 091601, arXiv:2004.02733 [hep-ph].

[46] G. Lucente, N. Nath, F. Capozzi, M. Giannotti, and A. Mirizzi, "Probing high-energy solar axion flux with a large scintillation neutrino detector," *Phys. Rev. D* **106** no. 12, (2022) 123007, arXiv:2209.11780 [hep-ph].

[47] L. Di Luzio *et al.*, "Probing the axion–nucleon coupling with the next generation of axion helioscopes," *Eur. Phys. J. C* **82** no. 2, (2022) 120, arXiv:2111.06407 [hep-ph].

[48] **Particle Data Group** Collaboration, R. L. Workman *et al.*, "Review of Particle Physics," *PTEP* **2022** (2022) 083C01.

[49] S. Hannestad, A. Mirizzi, and G. Raffelt, "New cosmological mass limit on thermal relic axions," *JCAP* **07** (2005) 002, arXiv:hep-ph/0504059.

[50] L. Di Luzio, G. Martinelli, and G. Piazza, "Breakdown of chiral perturbation theory for the axion hot dark matter bound," *Phys. Rev. Lett.* **126** no. 24, (2021) 241801, arXiv:2101.10330 [hep-ph].

[51] A. Notari, F. Rompineve, and G. Villadoro, "Improved hot dark matter bound on the QCD axion," arXiv:2211.03799 [hep-ph].

[52] L. Di Luzio, J. Martin Camalich, G. Martinelli, J. A. Oller, and G. Piazza, "Axion-pion thermalization rate in unitarized NLO chiral perturbation theory," arXiv:2211.05073 [hep-ph].

[53] L. Di Luzio, M. Fedele, M. Giannotti, F. Mescia, and E. Nardi, "Stellar evolution confronts axion models," *JCAP* **02** (2022) 035, arXiv:2109.10368 [hep-ph].

[54] A. Arvanitaki and A. A. Geraci, "Resonantly Detecting Axion-Mediated Forces with Nuclear Magnetic Resonance," *Phys. Rev. Lett.* **113** no. 16, (2014) 161801, arXiv:1403.1290 [hep-ph].

[55] A. Garcon *et al.*, "The Cosmic Axion Spin Precession Experiment (CASPEr): a dark-matter search with nuclear magnetic resonance," arXiv:1707.05312 [physics.ins-det].

[56] **LUX** Collaboration, D. S. Akerib *et al.*, "First Searches for Axions and Axionlike Particles with the LUX Experiment," *Phys. Rev. Lett.* **118** no. 26, (2017) 261301, arXiv:1704.02297 [astro-ph.CO].

[57] **PandaX-II** Collaboration, X. Zhou *et al.*, "A Search for Solar Axions and Anomalous Neutrino Magnetic Moment with the Complete PandaX-II Data," *Chin. Phys. Lett.* **38** no. 1, (2021) 011301, arXiv:2008.06485 [hep-ex]. [Erratum: Chin.Phys.Lett. 38, 109902 (2021)].

[58] **XENON** Collaboration, E. Aprile *et al.*, "Search for New Physics in Electronic Recoil Data from XENONnT," *Phys. Rev. Lett.* **129** no. 16, (2022) 161805, arXiv:2207.11330 [hep-ex].

[59] P. Sikivie, "Experimental Tests of the Invisible Axion," *Phys. Rev. Lett.* **51** (1983) 1415–1417. [Erratum: Phys.Rev.Lett. 52, 695 (1984)].

[60] A. Ayala, I. Dominguez, M. Giannotti, A. Mirizzi, and O. Straniero, "Revisiting the bound on axion-photon coupling from Globular Clusters," *Phys. Rev. Lett.* **113** no. 19, (2014) 191302, arXiv:1406.6053 [astro-ph.SR].

[61] O. Straniero, A. Ayala, M. Giannotti, A. Mirizzi, and I. Dominguez, "Axion-Photon Coupling: Astrophysical Constraints," in *11th Patras Workshop on Axions, WIMPs and WISPs*, pp. 77–81. 2015.

[62] M. Giannotti, I. Irastorza, J. Redondo, and A. Ringwald, "Cool WISPs for stellar cooling excesses," *JCAP* **05** (2016) 057, arXiv:1512.08108 [astro-ph.HE].

[63] M. Giannotti, I. G. Irastorza, J. Redondo, A. Ringwald, and K. Saikawa, "Stellar Recipes for Axion Hunters," *JCAP* **1710** no. 10, (2017) 010, arXiv:1708.02111 [hep-ph].

[64] O. Straniero, C. Pallanca, E. Dalessandro, I. Dominguez, F. Ferraro, M. Giannotti, A. Mirizzi, and L. Piersanti, "The RGB tip of galactic globular clusters and the revision of the bound of the axion-electron coupling," arXiv:2010.03833 [astro-ph.SR].

[65] M. Buschmann, C. Dessert, J. W. Foster, A. J. Long, and B. R. Safdi, "Upper Limit on the QCD Axion Mass from Isolated Neutron Star Cooling," *Phys. Rev. Lett.* **128** no. 9, (2022) 091102, arXiv:2111.09892 [hep-ph].

[66] P. Carenza, T. Fischer, M. Giannotti, G. Guo, G. Martínez-Pinedo, and A. Mirizzi, "Improved axion emissivity from a supernova via nucleon-nucleon bremsstrahlung," *JCAP* **10** no. 10, (2019) 016, arXiv:1906.11844 [hep-ph]. [Erratum: JCAP 05, E01 (2020)].

[67] E. W. Kolb and M. S. Turner, *The Early Universe*, vol. 69. 1990.

[68] R. H. Cyburt, B. D. Fields, K. A. Olive, and T.-H. Yeh, "Big Bang Nucleosynthesis: 2015," *Rev. Mod. Phys.* **88** (2016) 015004, arXiv:1505.01076 [astro-ph.CO].

[69] **Planck** Collaboration, N. Aghanim *et al.*, "Planck 2018 results. I. Overview and the cosmological legacy of Planck," *Astron. Astrophys.* **641** (2020) A1, arXiv:1807.06205 [astro-ph.CO].

[70] **Planck** Collaboration, N. Aghanim *et al.*, "Planck 2018 results. VI. Cosmological parameters," *Astron. Astrophys.* **641** (2020) A6, arXiv:1807.06209 [astro-ph.CO]. [Erratum: Astron.Astrophys. 652, C4 (2021)].

[71] **CMB-S4** Collaboration, K. N. Abazajian *et al.*, "CMB-S4 Science Book, First Edition," arXiv:1610.02743 [astro-ph.CO].

[72] **Simons Observatory** Collaboration, P. Ade *et al.*, "The Simons Observatory: Science goals and forecasts," *JCAP* **02** (2019) 056, arXiv:1808.07445 [astro-ph.CO].

[73] L. Caloni, M. Gerbino, M. Lattanzi, and L. Visinelli, "Novel cosmological bounds on thermally-produced axion-like particles," *JCAP* **09** (2022) 021, arXiv:2205.01637 [astro-ph.CO].

[74] F. D'Eramo, E. Di Valentino, W. Giarè, F. Hajkarim, A. Melchiorri, O. Mena, F. Renzi, and S. Yun, "Cosmological bound on the QCD axion mass, redux," *JCAP* **09** (2022) 022, arXiv:2205.07849 [astro-ph.CO].

[75] R. Z. Ferreira, A. Notari, and F. Rompineve, "Dine-Fischler-Srednicki-Zhitnitsky axion in the CMB," *Phys. Rev. D* **103** no. 6, (2021) 063524, arXiv:2012.06566 [hep-ph].

[76] **IAXO** Collaboration, A. Abeln *et al.*, "Conceptual design of BabyIAXO, the intermediate stage towards the International Axion Observatory," *JHEP* **05** (2021) 137, arXiv:2010.12076 [physics.ins-det].

[77] **IAXO** Collaboration, E. Armengaud *et al.*, "Physics potential of the International Axion Observatory (IAXO)," *JCAP* **06** (2019) 047, arXiv:1904.09155 [hep-ph].

[78] H. Georgi, D. B. Kaplan, and L. Randall, "Manifesting the Invisible Axion at Low-energies," *Phys. Lett. B* **169** (1986) 73–78.

[79] K. G. Chetyrkin, B. A. Kniehl, M. Steinhauser, and W. A. Bardeen, "Effective QCD interactions of CP odd Higgs bosons at three loops," *Nucl. Phys. B* **535** (1998) 3–18, arXiv:hep-ph/9807241.

[80] K. Choi, S. H. Im, and C. S. Shin, "Recent progress in physics of axions or axion-like particles," arXiv:2012.05029 [hep-ph].